WL-TR-91-4119

CHARACTERIZATION OF FRACTURE IN [0/90]3s SiC/1723 COMPOSITES

Demirkan Coker, Noel E. Ashbaugh
University of Dayton Research Institute
300 College Park
Dayton, Ohio 45469-0001

March 1992

Interim Report for Period August 1987 - September 1991

MATERIALS DIRECTORATE
WRIGHT LABORATORY
AIR FORCE SYSTEMS COMMAND
WRIGHT-PATTERSON AIR FORCE BASE, OHIO 45433-6533

NOTICE

When Government drawings, specifications, or other data are used for any purpose other than in connection with a definitely government-related procurement, the United States Government incurs no responsibility or any obligation whatsoever. The fact that the government may have formulated or in any way supplied the said drawings, specifications, or other data, is not to be regarded by implication or otherwise in any manner construed, as licensing the holder or any other person or corporation, or as conveying any rights or permission to manufacture, use, or sell any patented invention that may in any way be related thereto.

This report is releasable to the National Technical Information Service (NTIS). At NTIS, it will be available to the general public, including foreign nations.

This technical report has been reviewed and is approved for publication.

Jay R Jira

JAY R. JIRA
Project Engineer
Materials Behavior Branch
Metals and Ceramics Division

Katherine A. Williams

KATHERINE A. WILLIAMS
Technical Area Manager
Materials Behavior Branch
Metals and Ceramics Division

Allan W Gunderson

ALLAN W. GUNDERSON, Chief
Materials Behavior Branch
Metals and Ceramics Division

If your address has changed, if you wish to be removed from our mailing list, or if the addressee is no longer employed by your organization, please notify WL/MLLN, Wright-Patterson AFB OH 45433-6533 to help us maintain a current mailing list.

Copies of this report should not be returned unless return is required by security considerations, contractual obligations, or notice on a specific document.

REPORT DOCUMENTATION PAGE

Form Approved
OMB No. 0704-0188

1. AGENCY USE ONLY (Leave blank)	2. REPORT DATE	3. REPORT TYPE AND DATES COVERED
	March 1992	Interim / 27 Aug 87 - 17 Sep 91

4. TITLE AND SUBTITLE
Characterization of Fracture in $[0/90]_{3S}$ SiC/1723 Composites

5. FUNDING NUMBERS
F33615-87-C-5243
PE - 61102F
PR - 2302
TA - P1
WU - 02

6. AUTHOR(S)
D. Coker, N.E. Ashbaugh

7. PERFORMING ORGANIZATION NAME(S) AND ADDRESS(ES)
University of Dayton Research Institute
300 College Park
Dayton, Ohio 45469-0001

8. PERFORMING ORGANIZATION REPORT NUMBER
UDR-TR-91-64

9. SPONSORING/MONITORING AGENCY NAME(S) AND ADDRESS(ES)
Jay R. Jira (513) 255-1358
Wright Laboratory
Materials Directorate
Materials Behavior Branch (WL/MLLN)
Wright-Patterson Air Force Base, Ohio 45433-6533

10. SPONSORING/MONITORING AGENCY REPORT NUMBER
WL-TR-91-4119

11. SUPPLEMENTARY NOTES

12a. DISTRIBUTION/AVAILABILITY STATEMENT
Approved for public release; distribution unlimited.

12b. DISTRIBUTION CODE

13. ABSTRACT *(Maximum 200 words)*

The fracture behavior of $[0°/90°]_{3s}$ cross-plied ceramic-matrix composites is evaluated using compact tension specimens. The influence of notch preparation (abrasive water-jet or diamond saw cut) and fatigue precracking is investigated. The extent that a calculated critical stress intensity factor can be used as a fracture toughness parameter is investigated. The stress-intensity factor corresponding to the maximum load, K_{peak}, is found to yield consistent values for the precracked specimens. However, this parameter is found to be higher for precracked specimens than for notched specimens. This difference in K_{peak} is attributed to fiber bridging of the crack in the precracked specimens. No difference in material behavior is observed between specimens with abrasive water-jet and diamond saw notch extensions. There seems to be no noticeable size effects on K_{peak} for precracked specimens, in contrast with the uncracked specimens.

14. SUBJECT TERMS
Ceramic Matrix Composite, Fracture Toughness, Fatigue Precracking, Compact Tension, Linear Elastic Fracture Mechanics, Compliance, Crack

15. NUMBER OF PAGES
56

16. PRICE CODE

17. SECURITY CLASSIFICATION OF REPORT	18. SECURITY CLASSIFICATION OF THIS PAGE	19. SECURITY CLASSIFICATION OF ABSTRACT	20. LIMITATION OF ABSTRACT
UNCLASSIFIED	UNCLASSIFIED	UNCLASSIFIED	UL

ACKNOWLEDGEMENTS

The authors wish to thank the Materials Directorate, Wright Laboratory (WL/MLLN) at Wright-Patterson Air Force Base, Ohio for their support and for the use of their test equipment. The assistance of Dr. J. P. Gallagher for extensive review of the report and detailed discussion is gratefully acknowledged. The authors also like to thank Dr. T. Nicholas for reviewing the manuscript.

PREFACE

This report documents the investigation done on fracture toughness of SiC/1723 [0/90]3s crossplied composites. The research was conducted by Demirkan Coker and Noel E. Ashbaugh at the Wright Laboratory, Materials Directorate, Metals and Ceramics Division at Wright-Patterson Air Force Base, Ohio.

TABLE OF CONTENTS

LIST OF FIGURES

LIST OF TABLES

I INTRODUCTION

Ceramic matrix composites (CMCs) offer great promise as lightweight and strong materials for high performance structures operating at high temperatures. The potential applications of CMCs include gas turbine engines, components requiring resistance to aggressive environments, and special electronic/electrical applications. In these materials, ceramic matrices are toughened by incorporating SiC reinforcing fibers in them, thus exploiting the high temperature strength and environmental resistance of ceramic materials while lowering the risk of a brittle failure [1].

A major advantage of composites, compared with metals, is that the fiber-induced heterogeneity resists crack extension. In a fiber/matrix composite system, fibers tend to cause multiple small cracks and delay the formation of a large crack. The enhancement of local failures resulting from fiber breaking, matrix cracking, and interface debonding further reduces the energy level, and hence prevents catastrophic failure [2].

To predict such complex failure phenomena, accurate analytical models and verification experiments are required. Based on a literature survey, it can be concluded that there is a lack of reliable predictive procedures due to conflicting and insufficient experimental results. Available findings are discussed next.

Cruse and Konish [3] utilized ASTM E399 standard test for fracture toughness [4] for guidance to conduct toughness tests on a NARMCO graphite/epoxy composite system. They suggested that the metals-based fracture mechanics approach may be applied to $(0°/\pm45°/90°)_s$ laminates since behavior of these materials deviates from classic brittle behavior about the same extent as that of slightly ductile materials. The test data seem to warrant use of the metals-based approach to characterize the initiation of unstable crack growth. Cruse and Osias [5] reported the results of another test series and showed that

(i) a composite laminate may be characterized by a single value of fracture toughness, independent of specimen geometry and, to a lesser degree, specimen size; and

(ii) the fracture strength models presented in [5] for both angle ply and general orthotropic laminates are typically quite accurate in predicting experimental data.

For unidirectional composites, Slepetz and Carlson [6] have reported fracture toughness values, determined by the compliance calibration method, which were consistent with reported values obtained with other methods. However, they conclude that their fracture test does not seem to apply to cross-ply laminates because of the complex failure zone which develops in lieu of a sharp crack.

Marshall and Evans [7] have suggested that fracture mechanics can be applied to analyze failure in composites for each combination of composite and stress state. For composites, the major deviations from

linear elastic fracture mechanics are due to the mixed mode cracks and crack tip stresses that are functions of material properties and orientations. Parhizgar et al., [8] concluded that Linear Elastic Fracture Mechanics (LEFM) is applicable to cracks that grow along fibers, and for this case, a fracture toughness can be defined that is independent of crack length.

Wright and Iannuzzi [9] conducted tests on double edge notched specimens and concluded that LEFM can be used to describe failure of carbon reinforced epoxy specimens. Guess and Hoover [10] concluded that LEFM parameters are appropriate criteria for fracture if there is no delamination. They computed fracture toughness values which were dependent upon material constants but independent of crack length.

Phillips and Davidge [11] used a range of linear elastic fracture mechanics type specimens, such as edge notch, center notch, compact tension, etc., but the data were found to be dependent on geometry. Therefore the determined fracture toughness does not appear to be a true material property. The authors conclude that LEFM is not applicable to continuous fiber composites because of the complexity of failure, which is an unlocalized process, involving a multiplicity of cracks away from the major macroscopic separation zone. Modeling done by Lewis et al., [12] suggests that the stress required to propagate an opening mode crack in a composite is independent of crack length, negating the whole concept of crack toughness and its application to design and failure analysis. Luh and

Evans [13] conducted flexural tests on notched and precracked CMC specimens at room temperature which revealed delamination from the notch tip; at 1000°C, sharp cracks initiated from the notch and propagated in a plane normal to the applied tensile load. Ref. 13 implies that, while the high-temperature fracture may be characterized by a toughness parameter, a unique LEFM fracture toughness may not exist at room temperature.

The objective of this investigation was to study the fracture behavior of a NICALON/1723 ceramic composite and to evaluate the fracture toughness concepts. The program was also designed to evaluate the influence of specimen size and notch preparation on fracture behavior.

II MATERIAL AND TEST PROCEDURE

2.1 Material

This program utilized two panels of a NICALON/1723 glass-matrix composite, which were manufactured by Mr. Larry Zawada at the Wright Laboratory, Materials Directorate, Wright-Patterson Air Force Base. The composite was cross-plied with a $[(0°/90°)_3]_s$ lay-up. Panel thicknesses for the two panels were approximately 2.6 and 3.1 mm. The handbook elastic properties for the NICALON fiber and 1723 glass matrix are defined in Table 1 [14].

To obtain volume fraction of the fibers, V_f, a sample volume from a representative specimen was polished and photographed after failure of a specimen. V_f was then obtained by image processing. Fig. 1 shows a typical crosssection of the composite. An area consisting of only the cross-sectional view of the fibers was utilized for image processing. Depending on the size and location of the sample area selected, the V_f varied from 42-48%. The average fiber volume fraction for the plates was calculated to be 45%.

The composite modulus was analytically calculated by using rule of mixtures for the longitudinal and transverse plies averaged over the laminate. For 45% fiber volume fraction and for the constituent properties as given before, the modulus in the direction of the fibers was 138.4 GPa, and the modulus in the transverse direction to the

Table 1 Fiber and Matrix Handbook Properties of the Composite

	NICALON Fiber	1723 Glass-Matrix
Elastic Modulus (GPa)	180-200	88
Poisson's Ratio	0.3	0.22
CTE (/°C)	3.1 E-6	4.58 E-6

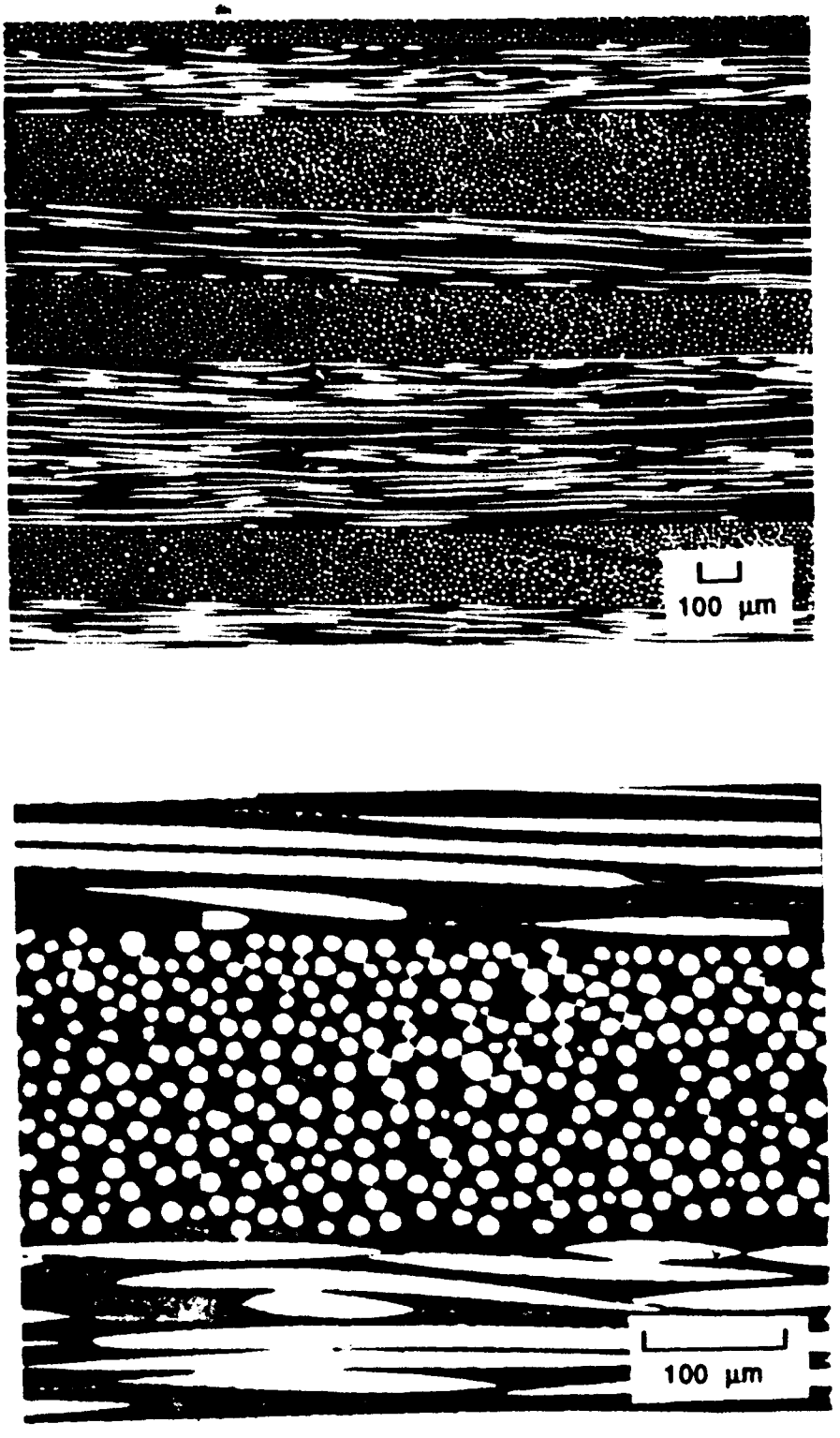

Fig. 1 Two microstructural Views of Mini C(T) 88C23-1

plies was 117.6 GPa. Since there were the same number of 0° and 90° plies in the laminate, the average was calculated to obtain the modulus of the composite as 128 GPa.

2.2 Specimen Geometry and Preparation

The test program utilized 5 standard compact (C(T)) specimens with a width of 40 mm and 12 mini compact specimens with a width of 20 mm. The C(T) specimen configuration is defined in Fig. 2 and the dimensions for the two C(T) specimen geometries (standard C(T) and mini C(T)) are presented in Table 2. The ASTM standard test E399 specifications were followed to design the specimen geometry except for the thicknesses which were taken as the available plate thicknesses (2.6 mm and 3.1 mm). The specimen locations in the two plates are shown in Fig. 3.

The pin holes in the standard C(T) were machined using abrasive water-jet while the pin holes for the mini C(T) specimens were drilled using a mandrel with the specimens sandwiched between wood plates to prevent delamination. The two methods yielded similar hole quality. Specimen notch extensions were produced by either abrasive water-jet (WJ), diamond-saw (DS) or fatigue precracking (FP). Notch tip radii for notches prepared with diamond-saw and abrasive water-jet were 0.009 mm and 0.008 mm, respectively. Fatigue precracking was conducted based on standard metal precracking procedures. For precracking, either constant

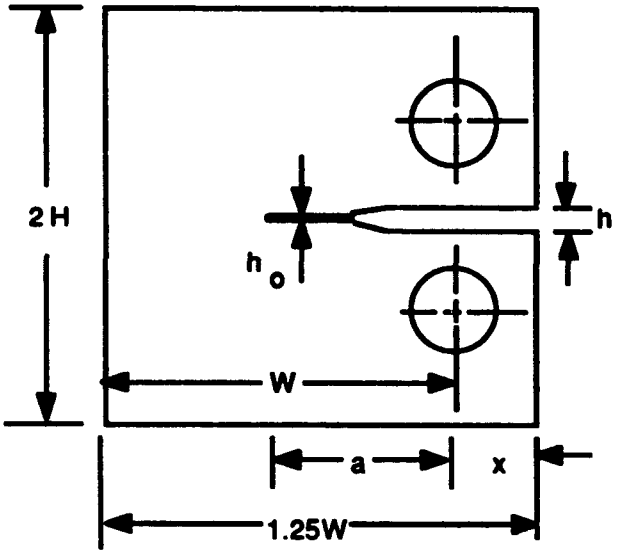

Definition of Terms

B : Thickness

W : Distance between load line and back face

H : Half height of specimen

h : Total height of notch slot

a : Distance between load line and notch tip

x_o : Distance between load line and front face

h_o : Height of extended slot

Fig. 2 Definition of Specimen Dimensions

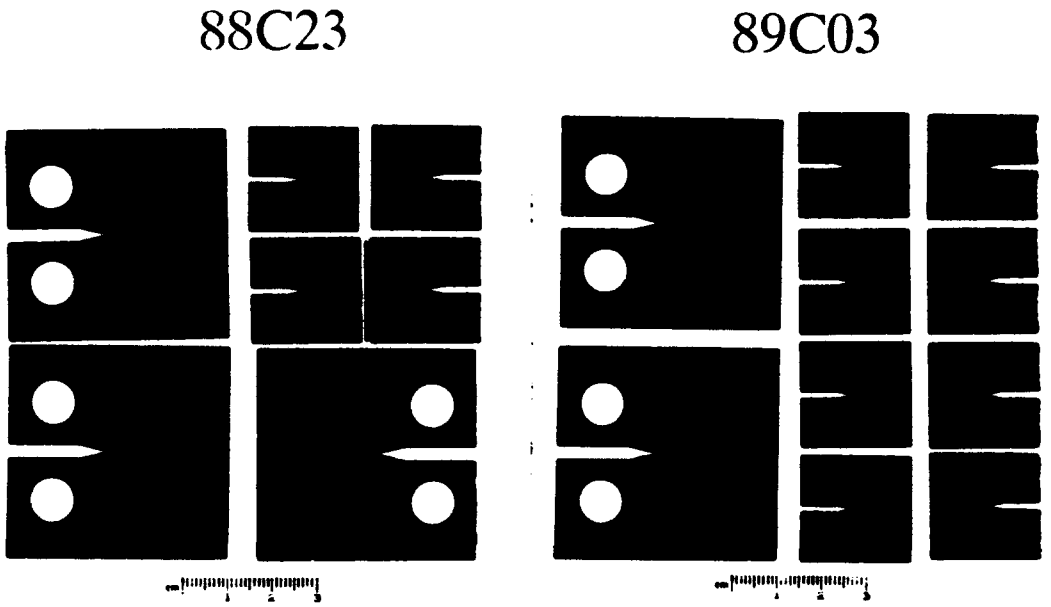

Fig. 3 Specimens Cut from Plates 88C23 and 89C03, Showing Initial Positions Within the Plate

Table 2 Specimen Dimensions

Specimen No.	Specimen Size*	B (mm)	W (mm)	H (mm)	xo (mm)	Notch Length (mm)	a/W
88C23-1	M	2.56	20.09	11.98	4.89	9.71	0.484
88C23-2	M	2.61	20.02	11.95	5.04	9.85	0.492
88C23-3	M	2.68	20.03	11.97	5.04	8.16	0.408
88C23-4	M	2.64	20.22	11.97	5.17	10.05	0.497
88C23-5	S	2.60	39.95	23.91	10.00	12.11	0.303
88C23-6	S	2.55	40.13	23.95	10.15	18.12	0.452
88C23-7	S	2.57	40.06	23.92	10.11	19.95	0.498
89C03-1	M	2.97	20.22	11.98	4.91	10.40	0.515
89C03-2	M	3.12	19.97	11.96	5.14	10.43	0.522
89C03-3	M	3.07	20.05	11.96	5.06	8.05	0.402
89C03-4	M	3.03	19.96	11.97	5.30	10.39	0.520
89C03-5	M	3.08	20.04	11.94	5.09	9.96	0.497
89C03-6	M	3.11	20.23	11.97	4.88	9.26	0.458
89C03-7	M	3.14	20.17	11.95	4.95	10.25	0.510
89C03-8	M	2.96	19.81	12.03	5.26	9.91	0.500
89C03-9	S	3.09	40.06	23.94	10.08	16.48	0.411
89C03-10	S	3.10	40.03	23.95	10.04	19.86	0.496

* M: Mini C(T), W = 20 mm
S: Standard C(T), W = 40 mm

maximum load control or constant maximum stress intensity factor control was used to extend the crack.

2.3 Test Procedures

The tests were conducted using an MTS servo-hydraulic machine with a 10 kN load cell under load rate control. The loading rate was 21 N/s to final failure. Crack mouth opening displacement (CMOD) was measured with a clip gage connected to knife edges glued onto the front face of the C(T) specimens.

The test matrix is shown in Table 3. Five specimens failed prematurely for various reasons, and 12 specimens provided acceptable results for understanding the materials fracture behavior. Three specimens were successfully fatigue-precracked and then tested. Eight specimens with abrasive water-jet notch extensions and six specimens with diamond-saw notch extensions were tested.

2.4 Compliance Crack Length Method

The composite modulus, E, was estimated experimentally for notched and precracked specimens from compliance using LEFM methods for isotropic materials. Results for compliance from Ref. 15 were revised to account for position of the clip gage and used to determine specimen modulus (see Appendix A for details). The composite moduli for the specimens, computed using the initial notch (crack) size compliance based on the Appendix A approach, are

Table 3 Test Matrix for the Determination of Fracture Toughness of NICALON/1723 Glass-Matrix Composite

SPECIMEN	SIZE°	NOTCH PREPARATION*			NOTES	a/W
		WJ	DS	FP		
88C23-1	M		X		[1]	0.484
88C23-2	M		X			0.492
88C23-3	M		X	X	[2]	
88C23-4	M	X				0.497
88C23-5	S			X	[1]	0.303
88C23-6	S		X	X	Controlled Pmax	0.525
88C23-7	S	X				0.498
89C03-1	M	X			[1]	0.515
89C03-2	M		X			0.522
89C03-3	M		X	X	Controlled Pmax	0.502
89C03-4	M		X			0.520
89C03-5	M		X			0.497
89C03-6	M		X	X	[2]	
89C03-7	M	X				0.510
89C03-8	M	X				0.500
89C03-9	S		X	X	Controlled Kmax	0.541
89C03-10	S	X				0.496

[1] failed at pin hole (corner specimen)

[2] failed at notch during precracking

* WJ : Abrasive Water-Jet
DS : Diamond-Saw
FP : Fatigue Precrack

° M: Mini C(T), W = 20 mm
S: Standard C(T), W = 40 mm

presented in Table 4. The average modulus for uncracked, notched specimens is computed to be 118 GPa and 129.8 GPa for the fatigue precracked specimens. This significant difference in moduli between the notched and precracked is attributed to the fact that fiber bridging exists in the precracked specimens, allowing for less displacement and tending to make the specimens stiffer for the same crack length. The moduli for notched specimens is consistent with results from investigations using other geometries. In Ref. 16, 119 GPa is reported for the composite modulus of an uncracked NICALON/1723 SEN (single edge notched) specimen, which is approximately the same as the modulus for the notched specimens used here.

2.5 Premature Failures

The specimen locations on the plates and premature failure observations are shown in Fig. 4. The mini C(T) specimens taken from the corners of each panel failed at the holes, due to matrix flowing out from the edges during consolidation of the composite and resulting in a strength loss in the corner region. For the same reason, one standard C(T) specimen at the corner (89C03-6) with no notch extension failed while attempting to fatigue precrack the sample at high load. To eliminate this problem, additional notch extensions were made to $a/W \approx 0.4$ in all other specimens to reduce high load levels which would cause failure at the holes.

Table 4 Estimates of Composite Modulus (E) Based on Eqn. A1

Specimen No.	Notch Extension*	Specimen Type**	B(mm)	W(mm)	a/W	x/W	C (mm/N)	E (GPa)
88C23-2	DS	M	2.61	20.02	0.492	-0.375	20.0	116.9
89C03-2	DS	M	3.12	19.97	0.522	-0.380	18.6	120.8
89C03-4	DS	M	3.03	19.96	0.520	-0.389	21.0	110.1
89C03-5	DS	M	3.08	20.04	0.497	-0.377	16.9	119.8
89C03-7	WJ	M	3.14	20.17	0.510	-0.367	17.1	121.4
89C03-8	WJ	M	2.96	19.81	0.500	-0.390	18.0	120.4
88C23-4	WJ	M	2.64	20.22	0.497	-0.378	21.0	112.9
89C03-3	PC	M	3.07	20.05	0.502	-0.252	14.2	126.9
88C23-6	PC	S	2.55	40.13	0.525	-0.253	17.5	137.5
89C03-9	PC	S	3.09	40.06	0.541	-0.252	17.1	125.0
88C23-7	WJ	S	2.57	40.06	0.498	-0.252	17.0	124.1
89C03-10	WJ	S	3.10	40.03	0.496	-0.251	15.0	116.0

* DS: Diamond-Saw Notch Extension
WJ: Abrasive Water-Jet Notch Extension
PC: Fatigue Precrack

** M: Mini C(T), W=20 mm
S: Standard C(T), W=40 mm

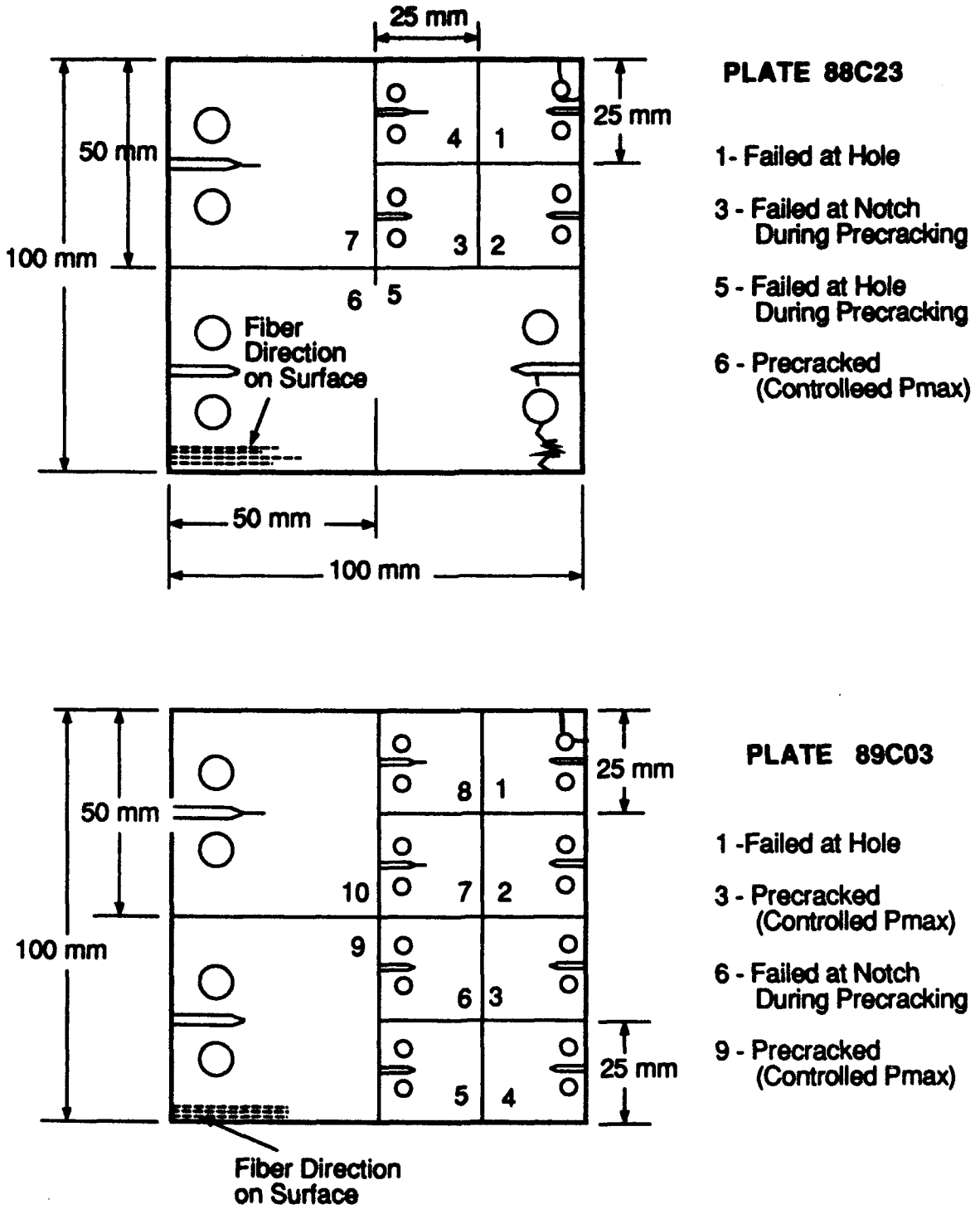

Fig. 4 Specimen Numbering Scheme for Panels 88C23 and 89C03 and Associated Premature Failures

Two mini compact tension specimens (W=20 mm) failed prematurely on the notch plane during fatigue precracking. This behavior was attributed to the corner cuts (Fig. 5) that may have caused delamination around the notch tip. The corners were cut to enlarge the notch width of the precracked mini C(T) specimen to fit the clip gage. This recourse was taken instead of taking measurements at a distance away from the front face because computations employed crack opening displacement at the front face of the C(T) specimen. In those tests with no precracking, it was not necessary to cut the corners at the front face.

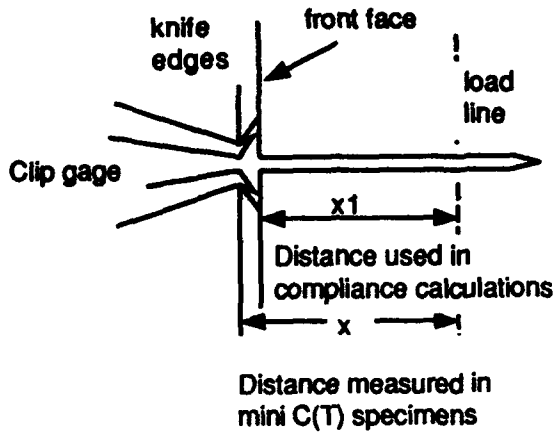

Initial Design

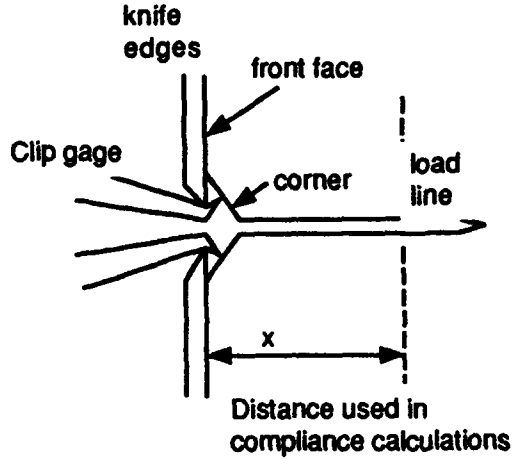

Modified Design

Fig. 5 Adjustments of the Knife Edges on the Front Face of the Mini C(T) Specimens

III RESULTS AND DISCUSSION

3.1 Precracking Behavior

One mini C(T) specimen (89C03-3) and two standard C(T) specimens (88C23-6 and 89C03-9) were successfully fatigue precracked. Crack lengths vs. cycle plots are presented in Appendix B. Optical crack lengths were acquired at several data acquisition cycles for comparison with calculated compliance crack length; these results are summarized in Fig. 6. The modulus used to obtain crack length estimates from compliance measurements was obtained from the first few cycles of the uncracked specimens.

Two measurements of crack length were made in specimen 89C03-9. Presented in Fig. 6, the lower measurement signifies the measured crack length in which the crack is assumed to extend only as far as the section that is opening and closing during cycles. The upper measurement signifies the crack length measured where the observable line extending from the crack is assumed to be the crack. Also presented in Fig. 6 are the crack length values for the other two precracked C(T) specimens (88C23-6, 89C03-3). As the crack length increases, the optical crack length exceeds the compliance crack length. This probably occurs because the optical readings are taken at the surface where extensive matrix cracking occurs. If the optical crack length is taken as the extent of observed relative movement of the crack, then the optical crack length value is even less than the

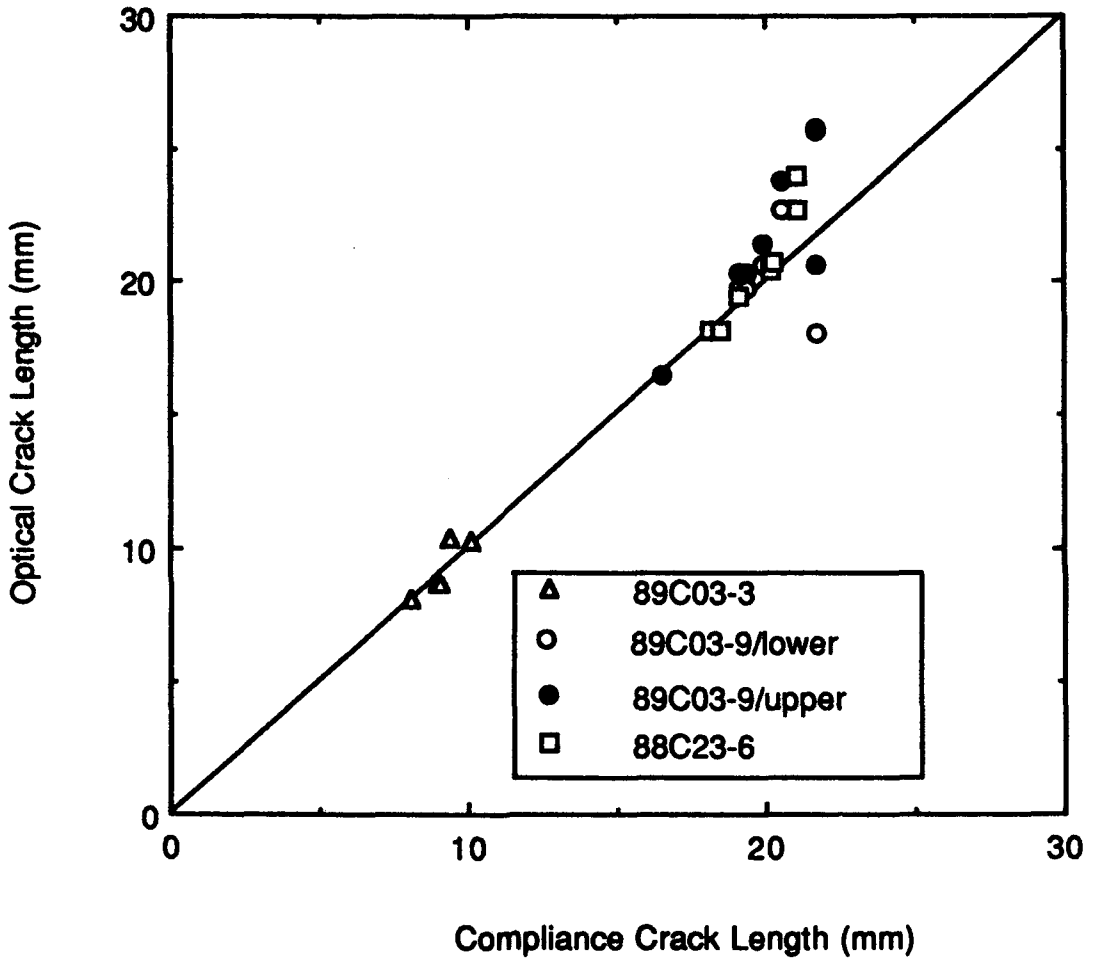

Fig. 6 Optical Crack Length vs. Compliance Crack Length for Precracked Specimens

compliance value (given by last two points in Fig. 6 for 89C03-9). Hence, it seems that the optical crack length measurement is not descriptive of the effective crack length. This point is further substantiated by the fracture surfaces which show more extensive fiber pull-out at the edges as discussed next.

3.2 Difference in Fracture Surfaces

Figures 7-9 show that the fracture surfaces of the fatigue precracked specimens exhibit more extensive fiber pull-out while fiber-matrix clumps are observed for the notched specimens. In all cases some fiber pullout occurs at the very beginning and also more fiber pull-out occurs near the edges extending as far as a/W=0.7. Figure 10 illustrates these effects schematically.

The fracture surfaces of precracked specimens show three distinct regions. There is an initial flat region ahead of the notch root where both the matrix and fibers are not sticking out of the plane of the crack. The second region is the excessive fiber pull-out region which levels off to the third region consisting of a flat surface with occasionally matrix-fiber clumps (Figures 7 and 8). In the case of notched specimens, there is a very limited fiber pull-out region near the notch-tip after which clumps of fiber and matrix are seen leveling off towards the end of the specimen (Fig. 9).

Fig. 7 Side View of Precracked Standard C(T) 89C03-9

Fig. 8 Side View of Precracked Mini C(T) 89C03-3

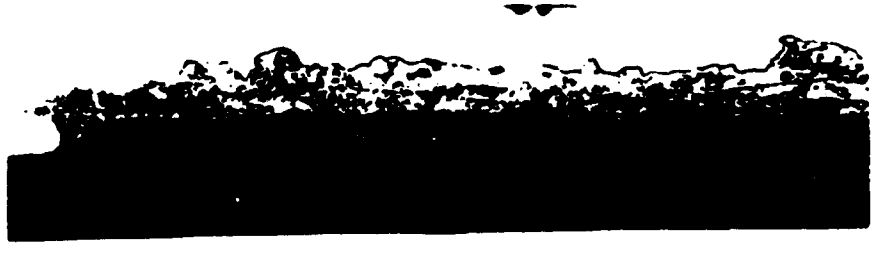

Fig. 9 Side View of Notched Mini C(T) 88C23-6

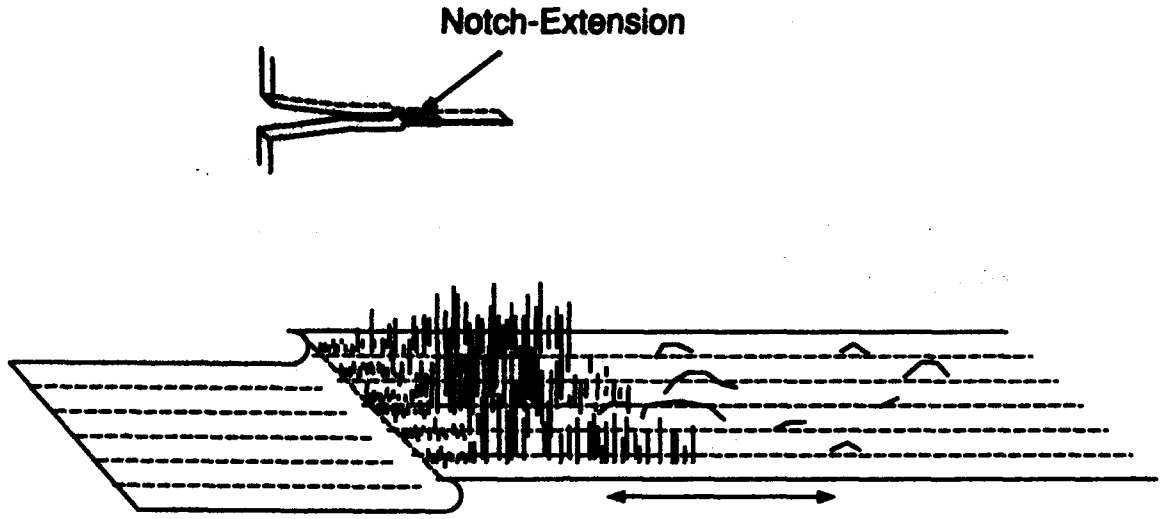

Precracked Specimen

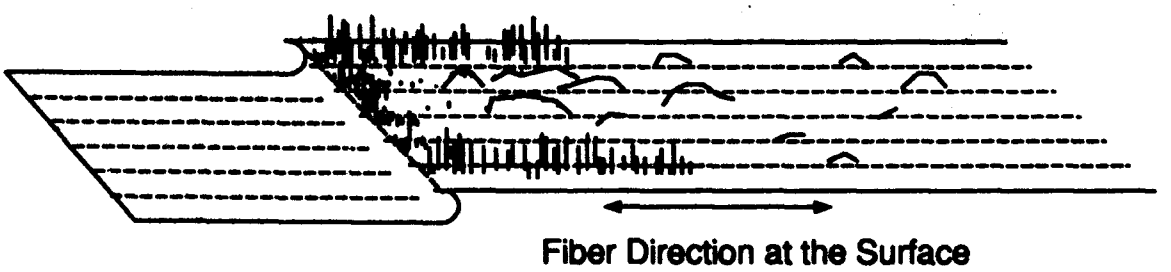

Notched Specimen

Fig. 10 Schematics of the Fracture Surfaces of Notched and Precracked Specimens

3.3 Load-Displacement Behavior

Two typical load-displacement traces obtained from the fracture tests are shown in Figures 11 and 12, for precracked and water-jet cut specimens, respectively. Appendix C presents the load displacement behavior for all the fracture tests. The general features of these curves are as expected for brittle matrix materials [17,18]. A typical curve initially consists of a linear region in which the specimen deforms elastically with an elastic modulus close to the rule of mixtures value. A second region of decreasing slope then begins as a result both of nonlinear load-displacement behavior of the composite (caused by the nonlinear behavior of the matrix under high loads) and of damage initiation by matrix cracking. Finally, the load peaks and falls off as the test piece breaks in two. Others have observed this same behavior in bend specimens with a very fine notch extension machined with an ultrasonic cutter [3,17].

The basic difference between the notched and the precracked specimens can be summarized in the typical load-displacement plot contours shown in Fig. 13. The load-displacement curves start with different slopes initially in the linear region. For the precracked specimens, the curve rises with a steeper angle which is almost constant and then levels off to a constant slope close to zero, displaying unstable crack propagation, and then failure. For no precrack, the slope changes gradually, reaching a maximum before the specimen fails.

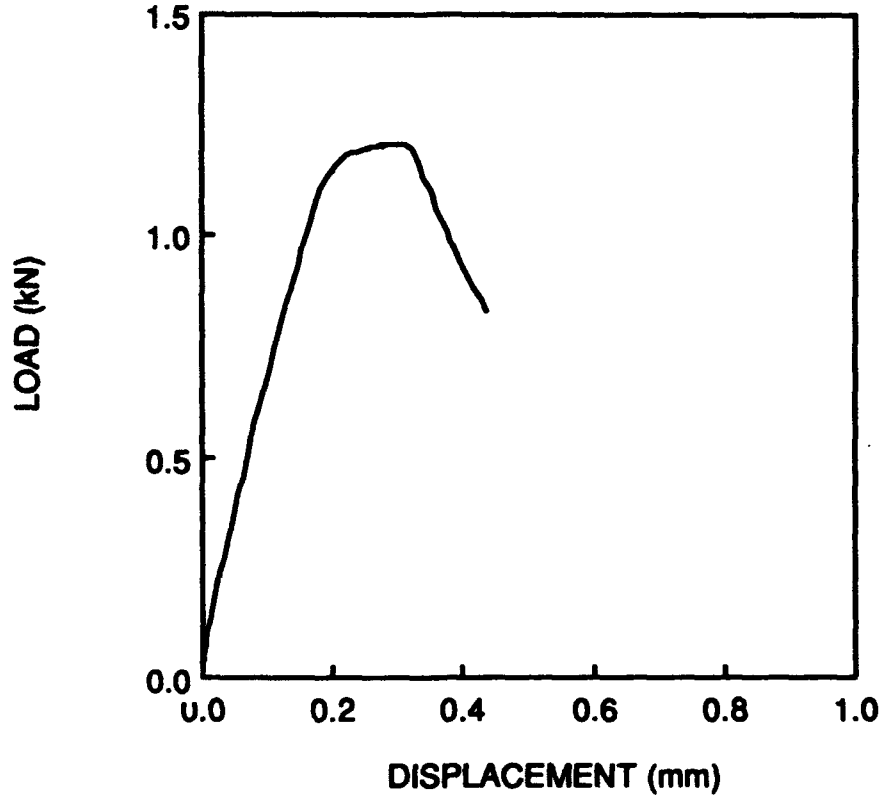

Fig. 11 Load Displacement Behavior of Specimen 89C03-3 (Mini, DS, precracked, a/W = 0.50)

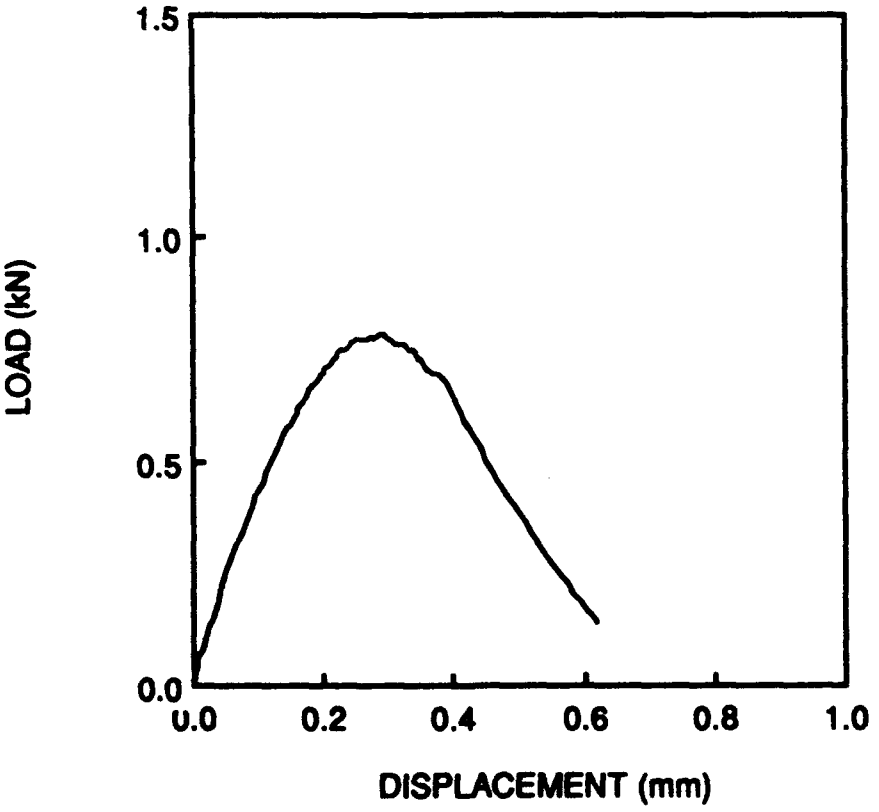

Fig. 12 Load Displacement Behavior of Specimen 88C23-4 (Mini, WJ notched, a/W = 0.50)

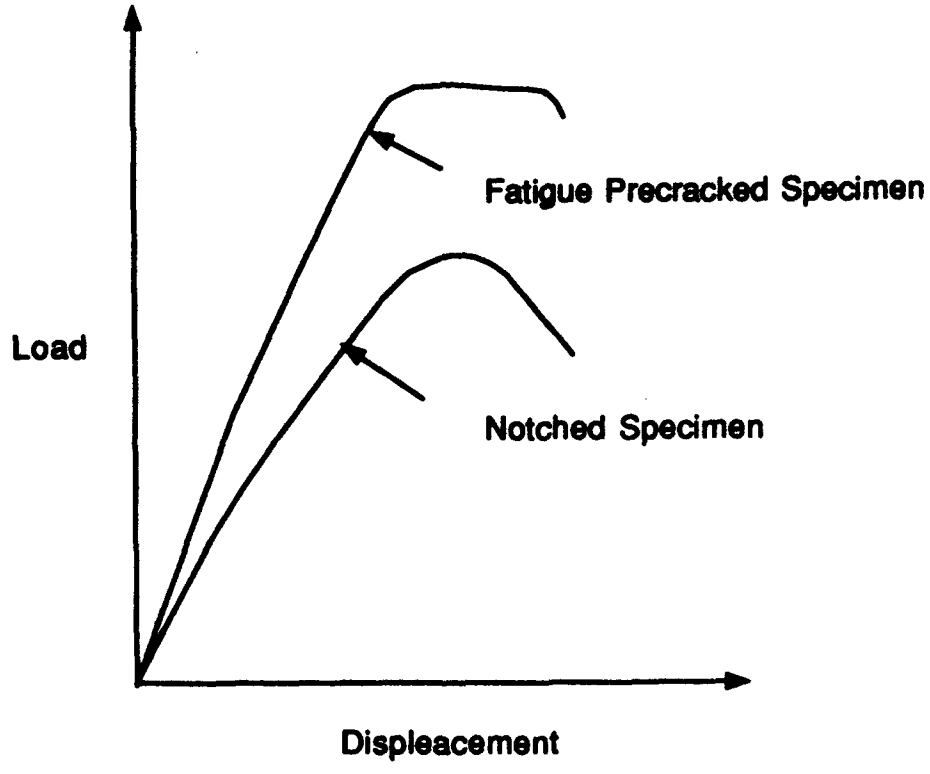

Fig. 13 Schematic of the Load-Displacement Behavior

3.4 Normalized Load-Displacement Curves

Load-displacement plots were normalized for notched and precracked specimens as shown in Figures 14-16. Figures 14 and 15 were normalized with respect to peak load and corresponding displacement. The overlapping of linear regions was expected for precracked specimens at the same a/W since the nondimensionalized compliance in the elastic region is dependent on a/W only, (thickness B and modulus E being kept constant). Interestingly, nonlinear effects seem to be the same for precracked specimens as opposed to that of notched specimens (Fig. 15). The plots of the three precracked specimens in Fig. 16 were normalized with respect to 40% of their peak load which corresponds to the linear region. Again the plots overlap. These three figures imply that the fracture behavior of cracked composites is distinctly different from the composites which were not precracked. Hence previous research that focused on observing and evaluating notch behavior of CMCs may not be appropriate to explain the fracture behavior of CMCs.

3.5 Estimates of Toughness

Table 5 summarizes the test results which include the elastic and peak loads and the corresponding stress intensity factors. Calculation of the stress intensity factor, K, was based on linear elastic fracture methods [4]. For a homogeneous, isotropic, linear-elastic material, K is related to the load by

$$K = P/(B\sqrt{W})*f(a/W)$$

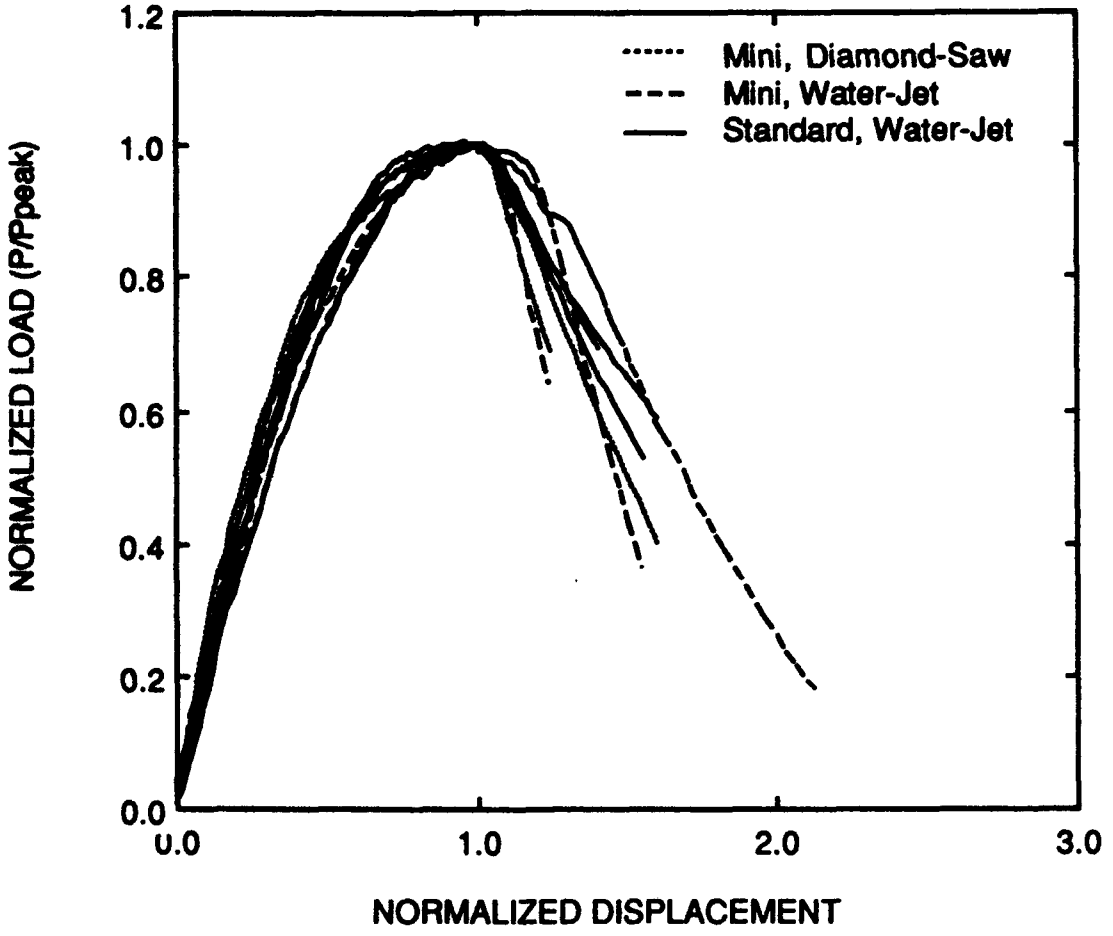

Fig. 14 Normalized Load-Displacement Plots for Notched Specimens (Normalized with respect to Peak Load and Its Corresponding Displacement)

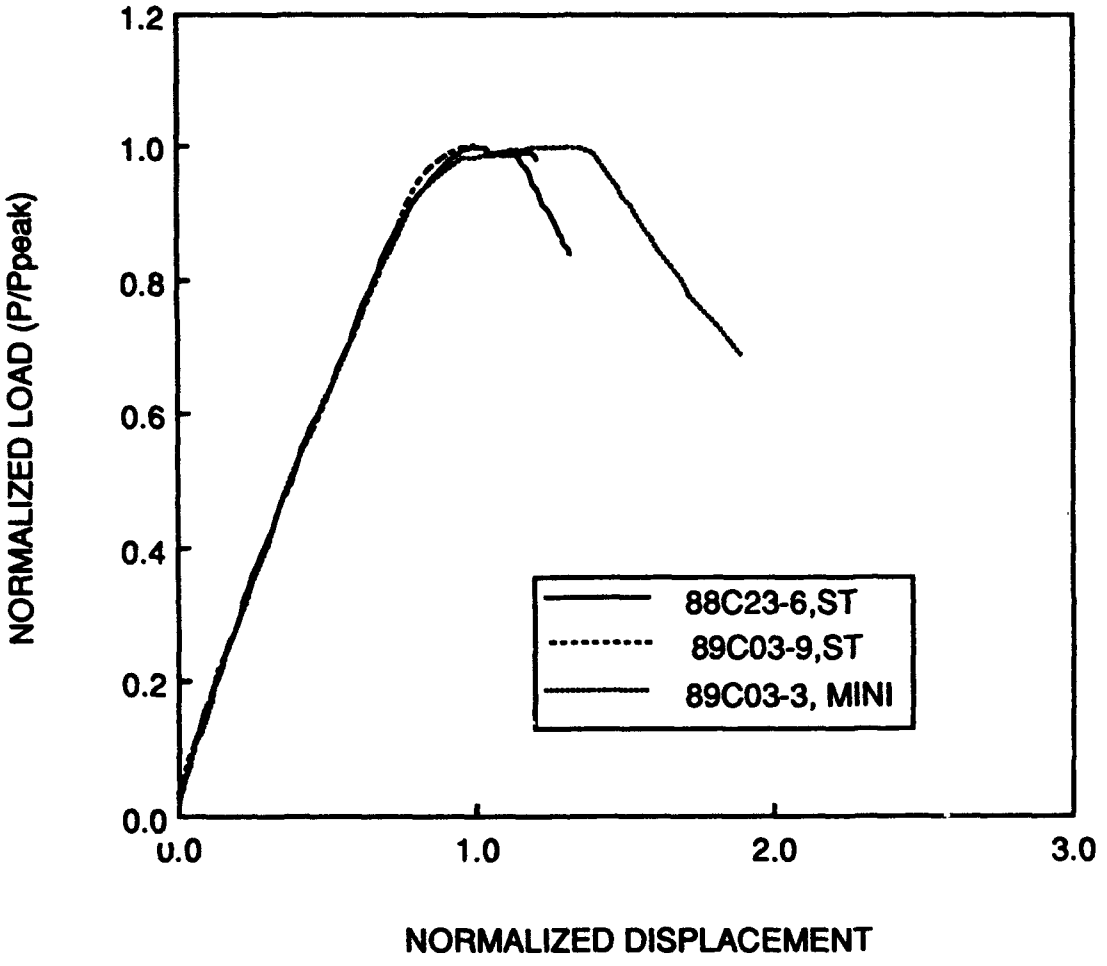

Fig. 15 Normalized Load-Displacement Plots for Precracked Specimens (Normalized with respect to Peak Load and Its Corresponding Displacement)

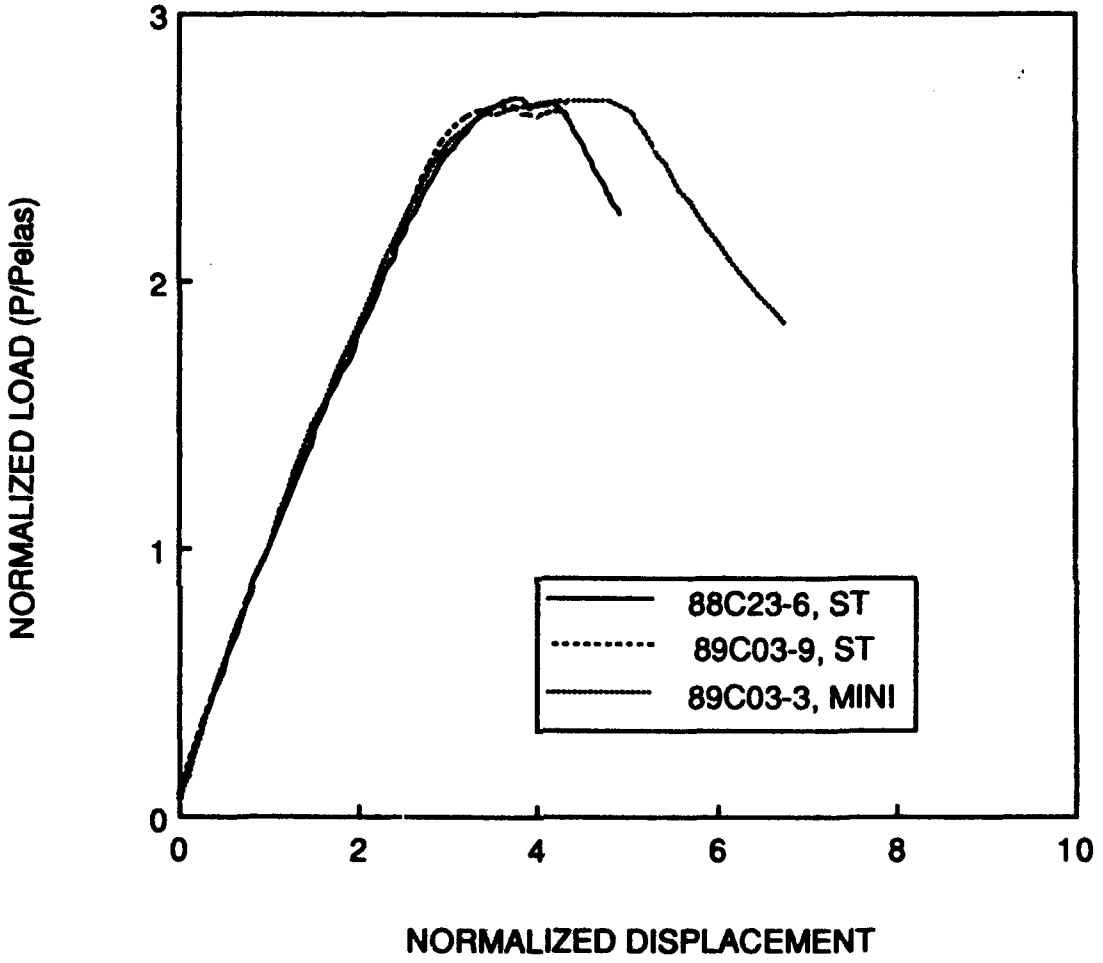

Fig. 16 Normalized Load-Displacement Plots for Precracked Specimens (Normalized with respect to Linear Load-Displacement Limit and Its Corresponding Displacement)

Table 5 Summary of Successful Tests for Fracture Toughness of NICALON/1723

Specimen No.	Notch Extension*	C(T) Type**	B(mm)	W(mm)	a/W	Pel (N)	Kel (MPa√m)	Pmax (N)	Kmax (MPa√m)
88C23-2	DS	M	2.61	20.02	0.492	287.4	7.3	827.5	21.1
89C03-2	DS	M	3.12	19.97	0.522	250.0	5.9	791.9	18.6
89C03-4	DS	M	3.03	19.96	0.520	168.6	4.0	818.6	19.6
89C03-5	DS	M	3.08	20.04	0.497	143.7	3.2	849.7	18.6
89C03-7	WJ	M	3.14	20.17	0.510	156.3	3.5	662.9	14.8
89C03-8	WJ	M	2.96	19.81	0.500	125.0	2.9	743.0	17.2
88C23-4	WJ	M	2.64	20.22	0.497	188.0	4.9	774.1	20.3
89C03-3	PC	M	3.07	20.05	0.502	156.3	3.5	1210.1	27.0
88C23-6	PC	S	2.55	40.13	0.525	250.0	5.1	1348.0	27.6
89C03-9	PC	S	3.09	40.06	0.541	312.7	5.6	1428.1	25.5
88C23-7	WJ	S	2.57	40.06	0.498	375.0	7.0	1227.9	22.9
89C03-10	WJ	S	3.10	40.03	0.496	281.3	4.3	1454.8	22.4

*DS: Diamond saw notch extension
WJ: Abrasive water jet notch extension
PC: Fatigue precracked
**M: Mini C(T), W=20 mm
S: Standard C(T), W=40 mm

where P is the load and f(a/W) is a geometry dependent function defined as

$$f(a/W) = \frac{(2+a/W)(0.886+4.64a/W-13.32(a/W)^2+14.72(a/W)^3-5.6(a/W)^4}{(1-a/W)^{3/2}}$$

for the C(T) geometry.

Stress intensity factor values corresponding to the elastic load and peak load that were calculated are shown in Fig. 17. There was no significant difference between the specimens with water-jet and diamond saw notch extensions. The major point of distinction of the fracture behavior was that between notched and precracked specimens. If we define K_{peak} to be the stress intensity factor corresponding to the peak load, then the average K_{peak} for notched specimens is calculated to be 19.5 MPa$\sqrt{m}$ and for the precracked specimens is calculated to be 26.7 MPa$\sqrt{m}$. Thus the K_{peak} for the precracked specimens is higher than K_{peak} for specimens with a blunt notch. This is contrary to what is seen in homogeneous metals. There are two interrelated explanations for this:

1) In a notched specimen, when a load is applied, a stress field is created around the crack tip which is distributed to the fibers through the matrix (Fig. 18). This stress field causes the fibers ahead of the crack to act under the effect of high stress concentration, causing them to break. In contrast, in a precracked specimen, there are fibers bridging the compliance crack. At the physical crack tip, the stress intensity factor is felt in the matrix and the fibers, whereas the bridging fibers are not affected by the stress intensity factor. These fibers prevent the crack from opening and propagating until a

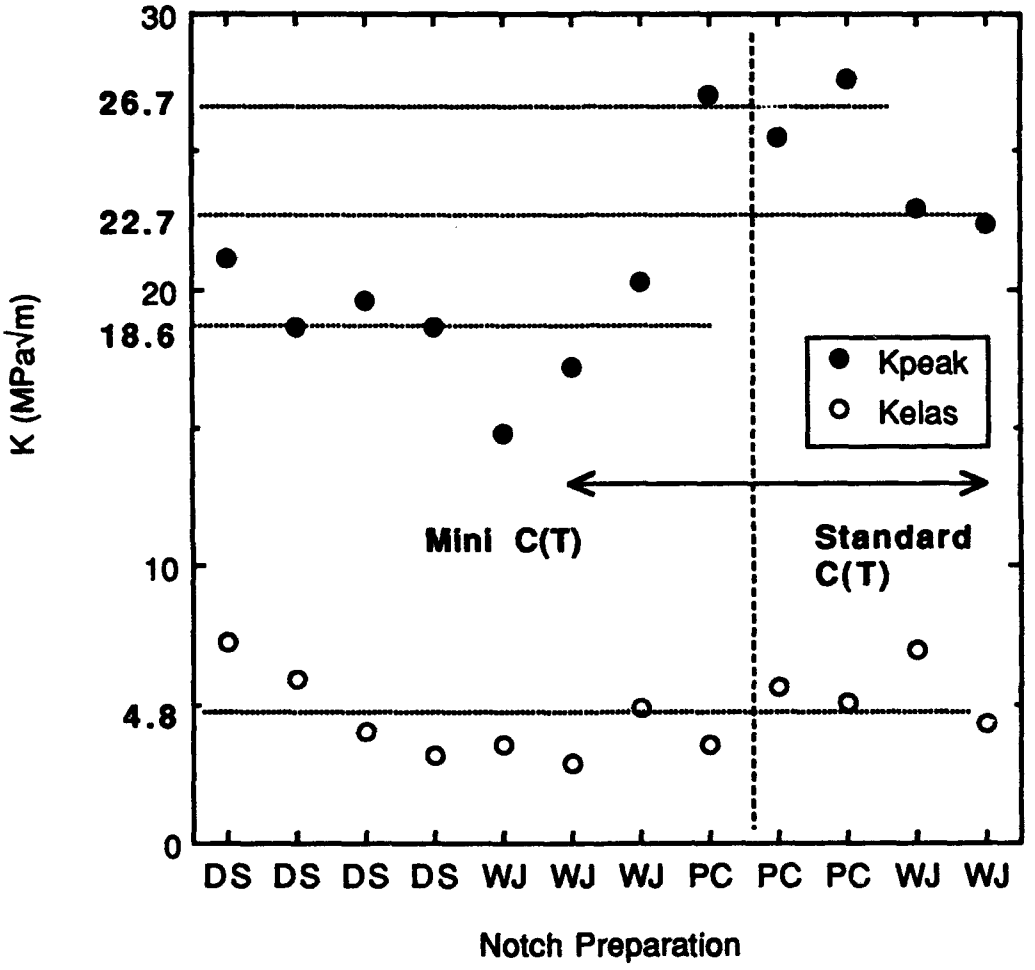

Fig. 17 Kpeak and Kelas for Specimens with Different Notch Extensions and Sizes (DS=Diamond Saw, PC=Precracked, WJ=Water Jet)

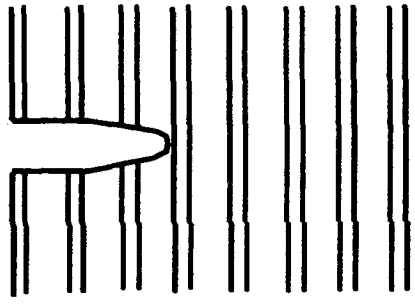

Notched Specimen

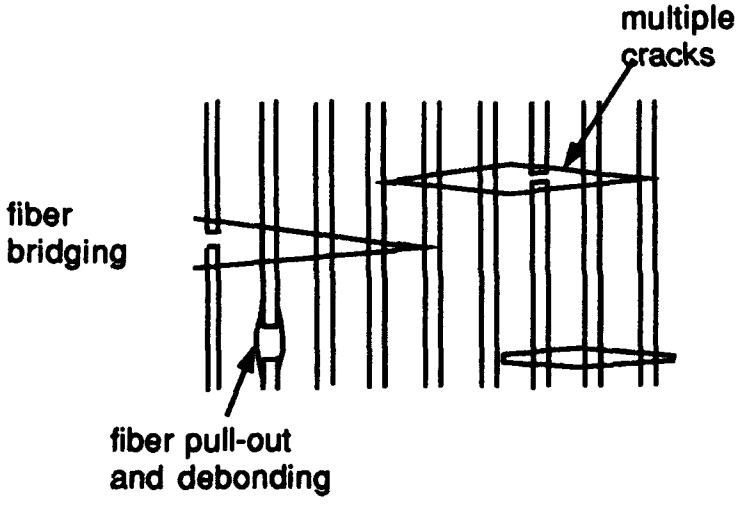

Precracked Specimen

Fig. 18 Schematic of Notch Tip and Failures Around a Crack Tip

critical load is reached and the bridging fibers start failing. In this case the calculated critical stress intensity factor does not only describe the local stress field around the crack tip, but also the effects of the ultimate strength or strain of the fiber.

2) During fatigue precracking, multiple cracking is seen. This reduces the energy density in the vicinity of the crack tip, hence the stress intensity factor, at the principal crack. Therefore, the material can withstand higher stress intensity factors or requires higher loads to create the same stress intensity factor.

There is also more consistency in the fatigue precracked specimen K_{peak} values. This may be due to the fact that a precracked specimen has a sharp crack while different notched specimens may have different root radii and imperfections dependent on the cut leading to fairly arbitrary load levels at which the crack starts propagating. While there seems to be a size effect on the stress intensity factor for notched specimens, this effect was not seen in precracked specimens (Fig. 17). Because of an insufficient number of samples and the scatter involved, further investigations are necessary to reach a conclusive result.

To calculate the fracture toughness corresponding to a load P_Q of a specimen, it is necessary to determine the point on the data curve which corresponds to the initiation of significant crack growth in that specimen. P_Q denotes a significant degradation of strength arising from the presence of an implemented flaw [15,16]. Following ASTM procedures, the 5% offset method was used for computation of K_5

from the load-displacement plots. The corresponding loads and stress intensity factors, tabulated in Table 6, are shown in Figures 19 and 20, respectively. The condition $P_{peak}/P_5 < 1.10$ is not satisfied. P_5 values were one-half to one-third of P_{peak}. As can be seen P_5 is still in the stable crack growth region. The five percent offset method used to determine the onset of unstable crack growth does not serve its purpose for this material. Ten and fifteen percent offsets were also used (Figures 19 and 20) and the results were inconclusive.

Observing the crack surface after fracture, it was conjectured that the effective crack length is at the end of fiber pull-out regions. These were measured with the microscope and the new crack lengths were determined. The new K_{peak} values using these new crack lengths were computed. Because the termination length of a fiber-pullout region is vague, no useful conclusions could be drawn. If the crack lengths were taken at the end of the fiber-matrix clumps instead of the fiber pull-out regions for notched specimens, the results were also inconclusive.

Table 6 Stress Intensity Factors Obtained with 5, 10 and 15 Percent Offset Methods

Specimen No.	Notch Extension*	C(T) Type**	W(mm)	a/W	P5 (N)	K5 MPa√m	P10 (N)	K10 MPa√m	P15 (N)	K15 MPa√m
88C23-2	DS	M	20.02	0.492	413	10.52	475	12.12	563	14.35
89C03-2	DS	M	19.97	0.522	388	9.10	500	11.75	569	13.36
89C03-4	DS	M	19.96	0.520	313	7.50	369	8.85	481	11.54
89C03-5	DS	M	20.04	0.497	300	6.58	363	7.95	463	10.14
89C03-7	WJ	M	20.17	0.510	344	7.65	369	8.21	450	10.02
89C03-8	WJ	M	19.81	0.500	288	6.66	400	9.27	488	11.30
88C23-4	WJ	M	20.22	0.497	389	10.21	400	10.49	531	13.92
89C03-3	PC	M	20.05	0.502	375	8.38	588	13.13	775	17.32
88C23-6	PC	S	40.13	0.525	438	8.95	500	10.23	781	15.98
89C03-9	PC	S	40.06	0.541	625	11.14	825	14.71	1300	23.18
88C23-7	WJ	S	40.06	0.498	594	11.08	700	13.06	813	15.16
89C03-10	WJ	S	40.03	0.496	594	9.14	781	12.02	1019	15.69

*DS: Diamond saw notch extension
WJ: Abrasive water jet notch extension
PC: Fatigue precracked
**M: Mini C(T), W=20 mm
S: Standard C(T), W=40 mm

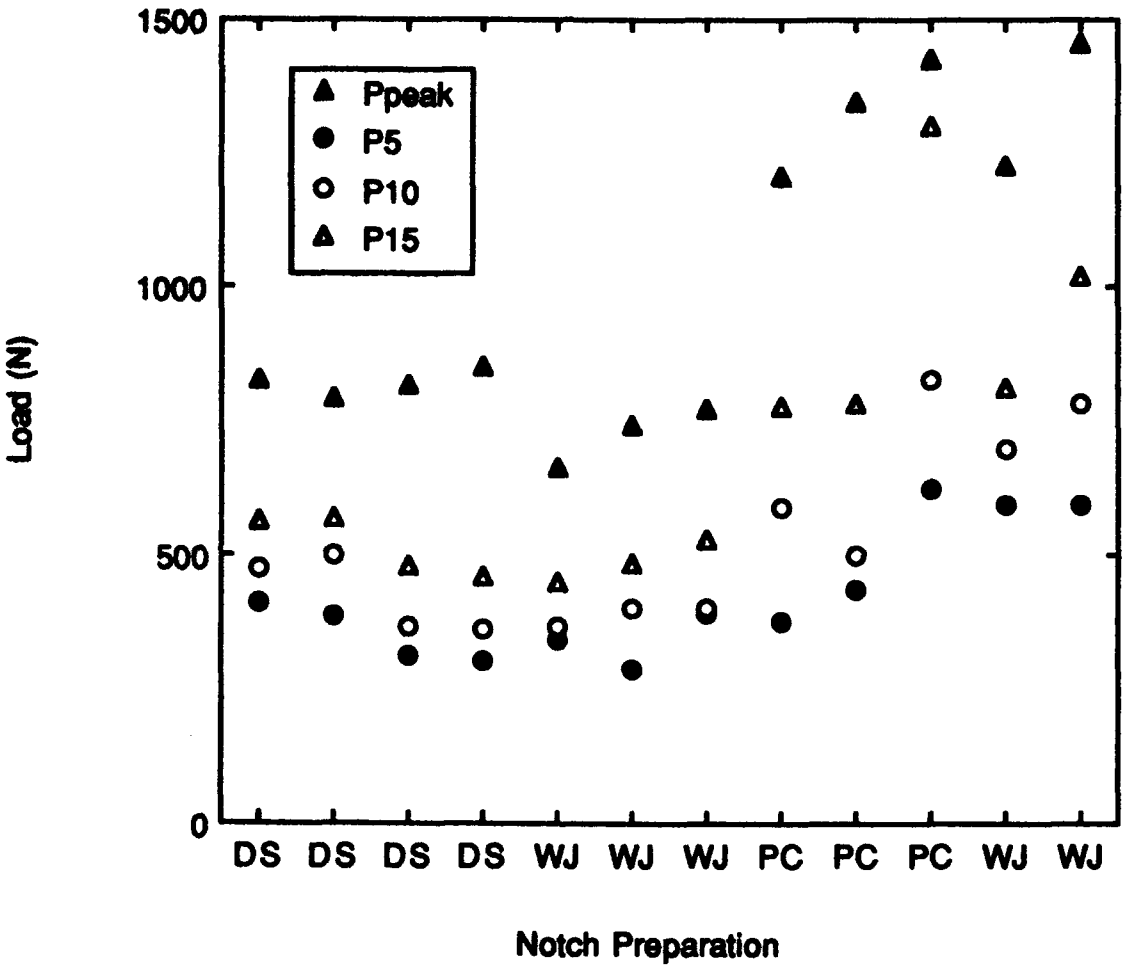

Fig. 19 Load Corresponding to 5, 10 and 15 Offset Methods and Peak Load

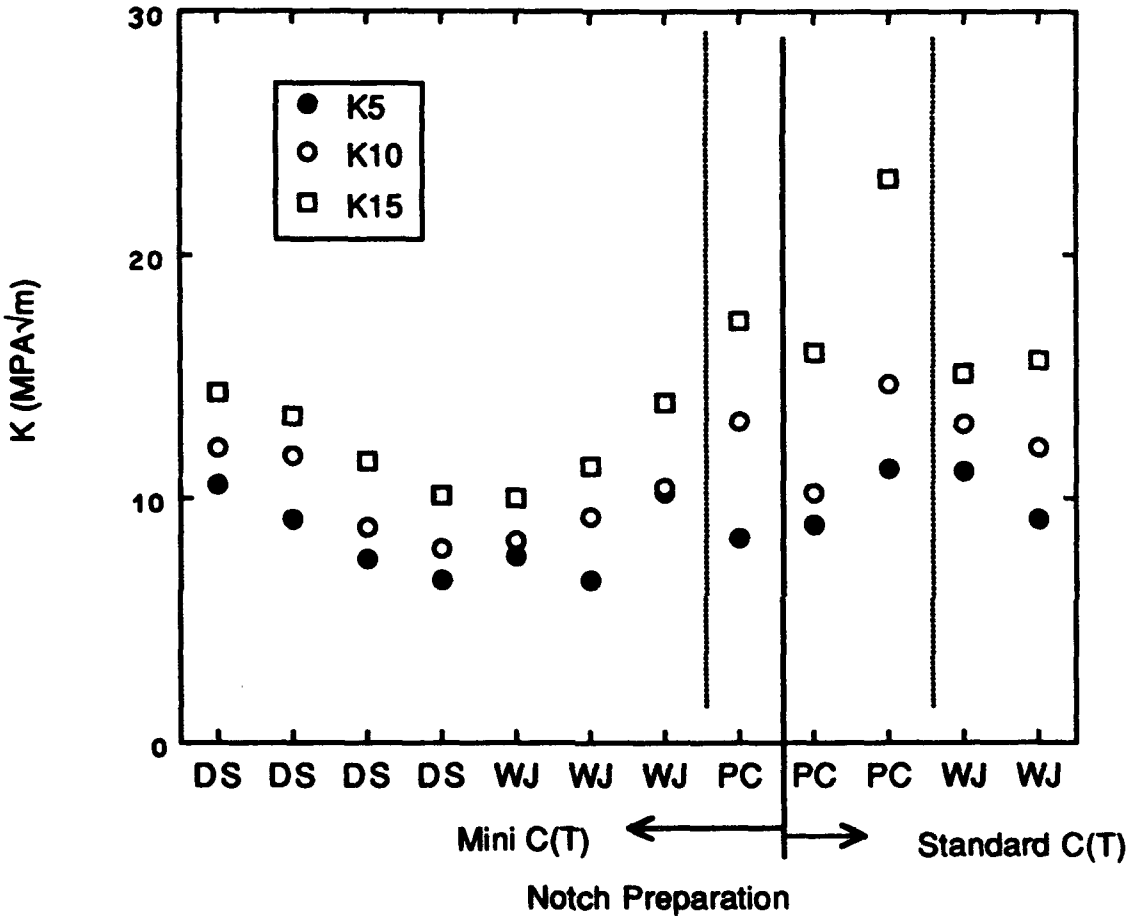

Fig. 20 Plots of K5, K10, K15 for Different Notch Preparations

IV CONCLUSIONS

The fracture behavior of cross-plied ceramic-matrix composites was evaluated using 10 mm and 20 mm C(T) specimens. Notch sharpness was evaluated using diamond-saw or abrasive water-jet techniques as compared to fatigue precracking. The specimens were monotonically loaded until fracture occurred and load-crack opening displacements plots were obtained.

The conclusions drawn from this investigation are:

1) A distinct difference exists between the fracture behavior of precracked and notch extended specimens. This difference was noticeable in fracture surfaces and load-displacement plots for monotonic loading. For precracked specimens, there was a decreased constant-slope region towards the end of monotonic loading which may correspond to frictional pull-out of broken fibers.

2) The stress intensity factor calculated at the peak load (K_{peak}) may be a suitable candidate for a fracture toughness value instead of the K_5 which does not correspond to the onset of unstable crack propagation. For fatigue precracked specimens consistent K_{peak} values were obtained. These K_{peak} values were approximately 30% higher than those of the notched specimens.

3) No difference in material behavior was observed between water-jet cut and diamond saw notch extensions. While there seems to be a tendency for size dependency of notched specimens, no noticeable size effects on K_{peak} for precracked specimens were observed.

4) Crack growth behavior differs from that of metallic materials. The precracking tests, which can be considered preliminary crack growth rate tests, show that the cracks sometimes arrest at constant P_{max} or K_{max} following an initial accelerated crack growth.

5) Load-displacement behavior resembles inelastic material behavior.

6) The fracture behavior of precracked CMCs appears to be more consistent than that of the notched specimens. Hence results obtained by previous investigations from unprecracked specimens may not yield consistent results with respect to nonlinear behavior and size independence.

REFERENCES

[1] Chawla, K. K., Composite Materials-Science and Engineering, Springer-Verlag, New York, 1987

[2] Sih, G. C., ed., Mechanics of Fracture-6, Cracks in Composite Materials, Martinus Nijhoff Publishers, 1981

[3] Cruse, T. A. , Konish, H. J., Jr.,"Elastic Fracture Mechanics for Advanced Fiber Composites: A Macromechanics Treatment," Polymer-Plastic Techno. Eng., 4 (1), pp. 41-91, 1975

[4] "Standard Method of Test for Plane-Strain Fracture Toughness of Metallic Materials," ASTM designation E399-83, Vol. 03-01, 1983, ASTM Annual Standards, American Society for Testing and Materials

[5] Cruse, T. A. and J. R. Osias, "Exploratory Investigations on Fracture Mechanics of Composite Materials," AFML-TR-74-11, April, 1974

[6] Slepetz, J. M. and Carlson, L., "Fracture of Composite Compact Tension Specimens," Fracture Mechanics of Composites, ASTM STP 593, American Society for Testing and Materials, pp. 143-162, 1975

[7] Marshall, D. B. and Evans, A. G., "Application of Fracture Mechanics to Fiber Composites," Ceramic Proceedings-Engineering and Science, pp. 527-539, July-August, 1985

[8] Parhizgar, S., Zachary, L. W., and Sun, C. T., "Application of the Principles of Linear Fracture Mechanics to the Composite Materials," International Journal of Fracture, Vol. 20 , pp. 3-15, 1982

[9] Wright, M. A. and Iannuzzi, F. A., "The Application of the Principles of Linear Elastic Fracture Mechanics to Unidirectional Fiber Reinforced Composite Materials," J. Composite Materials, Vol. 7, pp. 430-447, October, 1973

[10] Guess, T. R. and Hoover, W. R., "Fracture Toughness of Carbon-Carbon Composites," J. Composite Materials, 7, pp. 2-20, 1973

[11] Phillips, D. C. and Davidge, R. W., "Test Techniques for the Mechanical Properties of Ceramic Matrix Fiber Composites," AERE-G 3693, Not for Publication, October, 1985

[12] Lewis, D., et al., "Standard Testing of Refractory Matrix/Ceramic Fiber Composites," Ceramic Proceedings - Engineering and Science, pp. 507-510, July-August, 1985

[13] Luh, E. Y. and Evans, A. G., "High-Temperature Failure of a SiC fiber- reinforced LAS Glass Ceramic," Ceramic Proceedings-Engineering and Science, pp. 608-611, July-August, 1985

[14] Cornie, J. A., Chiang, Y., Uhlmann, D. R., Mortensen, A. and Colins, J. M., "Processing of Metal and Ceramic Matrix Composites," Ceramic Bulletin, vol. 65, no 2, pp. 293-304, 1986

[15] Saxena, A. and Hudak, S. J., Jr, "Review and Extension of Compliance Information for Common Crack Growth Specimens," International Journal of Fracture, Vol. 14, No 5, October, 1978

[16] Ashbaugh, N. E., Khobaib, M., Hartman, G. A., Coker, D., Kroupa, J. L., John, R., Johnson, D. A., Goodman, R. C., Maxwell, D. C., Muhic, L. A., Mechanical Properties for

Advanced Engine Materials - 1989 Annual Report, UDR-TR-90-85, August, 1990

[17] Barsom, J. M., Rolfe, S. T., Fracture and Fatigue Control in Structures - Applications of Fracture Mechanics, Prentice-Hall, New York, 1987

[18] Konish, H. J., Jr., Swedlow, J. L. and Cruse, T. A., "Experimental Investigations of Fracture in an Advanced Fiber Composite," Journal of Composite Materials, Vol. 6, p. 114, January 1972

APPENDIX A

COMPLIANCE CALCULATIONS

The composite modulus, E, can be estimated experimentally from compliance using linear elastic fracture mechanics methods. In Ref. 15, EBC, the nondimensional compliance for homogeneous and isotropic metals, is tabulated as a function of a/W, for different x/W where x is the distance from the load line where the clip gage is located, a is the crack or notch length, E is the elastic modulus, B is the thickness of the specimen, and C is the compliance determined from the load-displacement plots. Ref. 15 results for compliance could not be directly utilized for this test program because position of the clip gage was not the same for each specimen. The reason for this was that the composite was very sensitive to cutting out sharp corners because of delamination. Therefore knife edges could not be machined integral with the specimen but instead attachable knife edges were fixed to the specimen with super glue. This arrangement changed the position of the clip gage, which was attached to the knife edge, with respect to the load line (x/W).

In Fig. A1, linear equations are fitted to Saxena-Hudak data of EBC vs. x/W resulting in:

$$EBC = a + b\ x / W \qquad (A1)$$

where a and b both are functions of a/W. Three equations were setup for three different a/W ratios: 0.45, 0.50, 0.55. In Fig. A2, quadratic

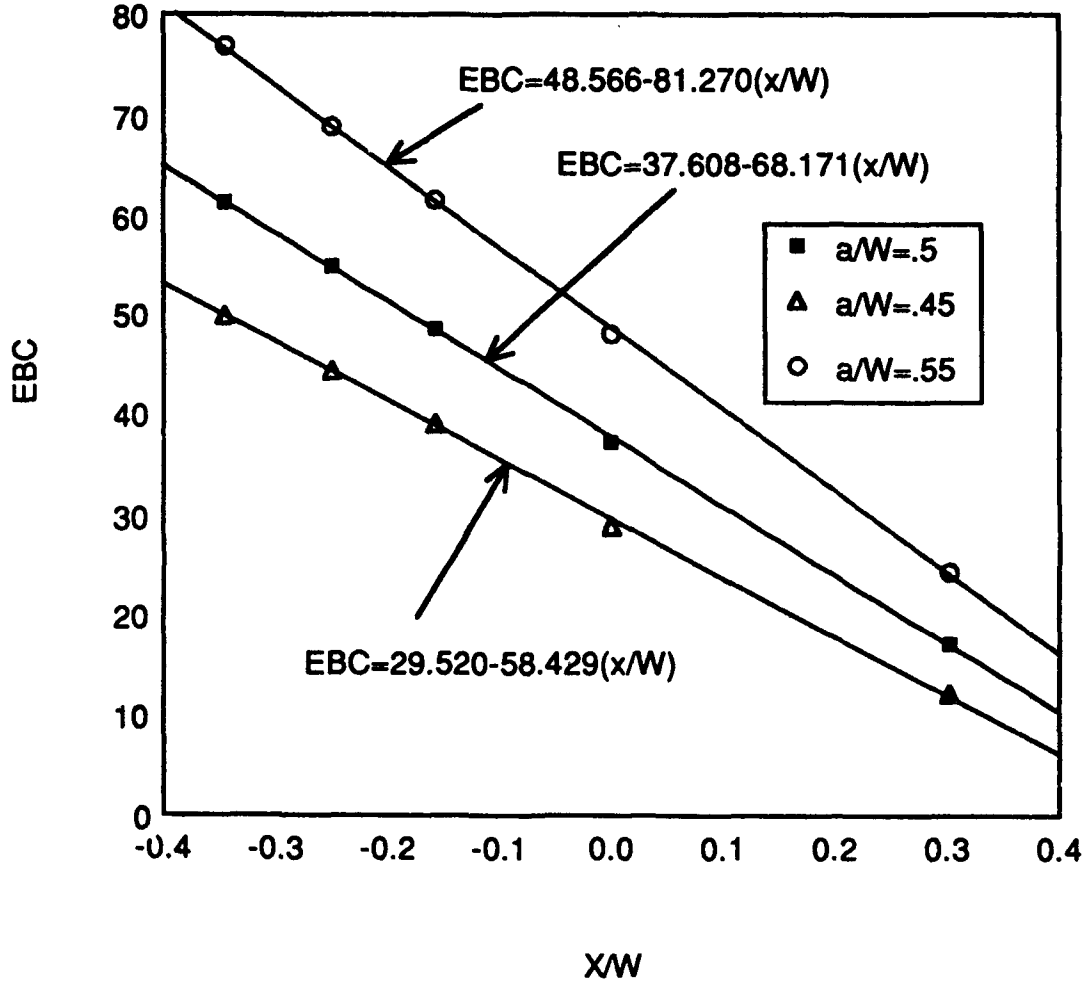

Fig. A1 EBC as a Function of Position (x/W) for $0.4 < a/W < 0.6$ (Data from Ref. 11)

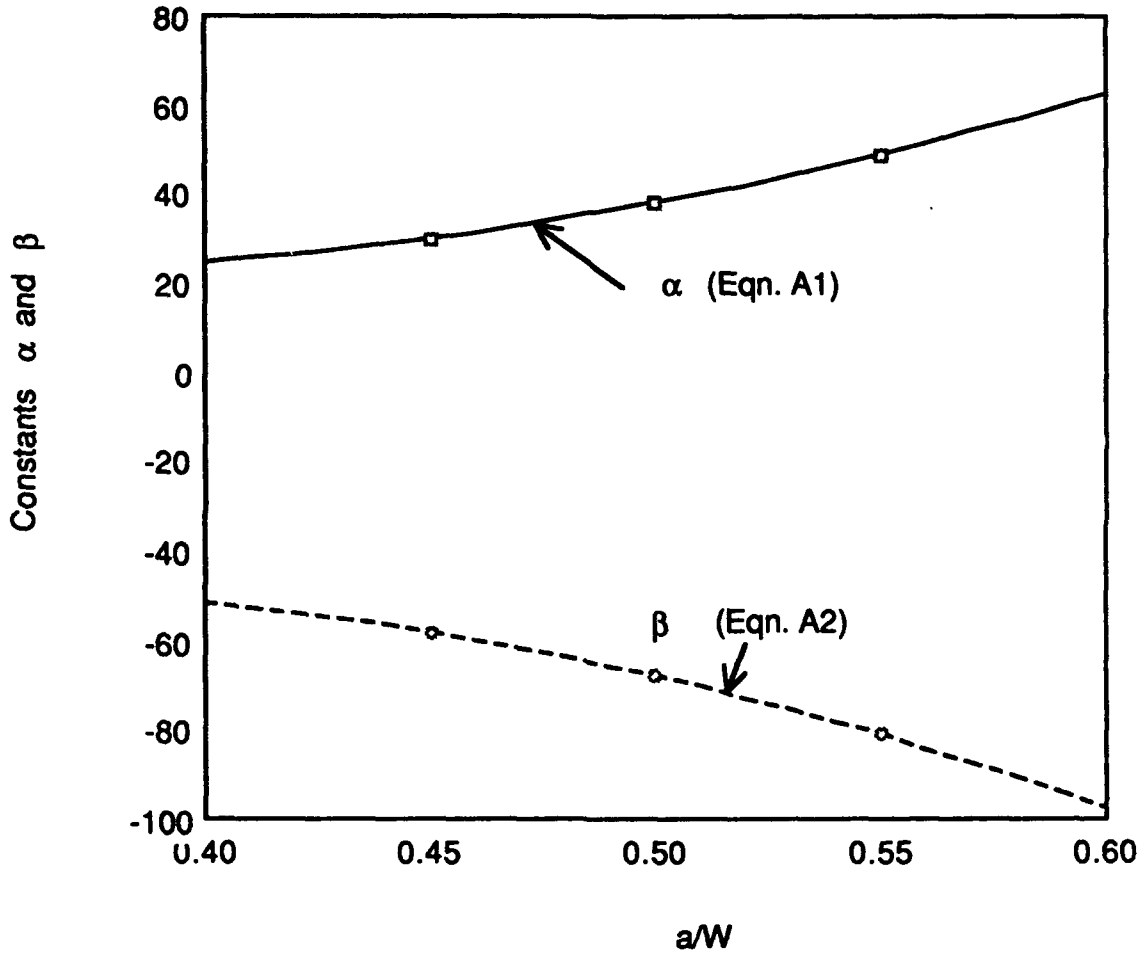

Fig. A2 EBC as a Function of a/W Based on Linear Models Presented in Figure A1

equations are curve fit to the coefficients a and b for varying a/W ($0.4 \leq a/W \leq 0.6$). The resulting polynomials for the constants were:

$$a = 85.878 - 383.54\,(a/W) + 574\,(a/W)^2 \qquad (A2)$$

$$b = -121.82 + 442.99\,(a/W) - 671.4\,(a/W)^2 \qquad (A3)$$

For a given notch size (or crack size) a/W, thickness B, the compliance C was measured and then the composite modulus, E, was estimated.

APPENDIX B

PRECRACKING HISTORY

Precracking history for standard C(T) specimen 88C23-6 is shown in Fig. B1. Fatigue precracking was started with a constant (low) maximum load under load control. After some crack propagation, crack arrest was observed at this load. The load was increased to a higher constant value. After some additional crack propagation, crack arrest occurred again. This phenomenon repeated until, by increasing the constant load, K_{max} reached the neighborhood of K_{peak} established from the tests on notched specimens. After reaching this critical value, the crack started jumping in discrete steps after very short crack slowdown intervals without any load increase. The precracking was completed when the final precrack size was reached.

Similar behavior was seen in the fatigue precracking of the other two specimens, standard C(T), 89C03-9, shown in Fig. B2, and mini C(T), 89C03-3, shown in Fig. B3. The load was increased constantly for 88C23-6 because precracking was started with a low K_{max} while the precracking for the other two specimens was started with a high load corresponding to a stress intensity factor close to K_{peak} of the notched specimens. Specimen 89C03-9 was tested under controlled maximum load starting with a high K_{max}. There was no crack propagation, optical or compliance, until the stress intensity factor was increased to approximately 21 MPa$\sqrt{m}$. At a stress intensity factor

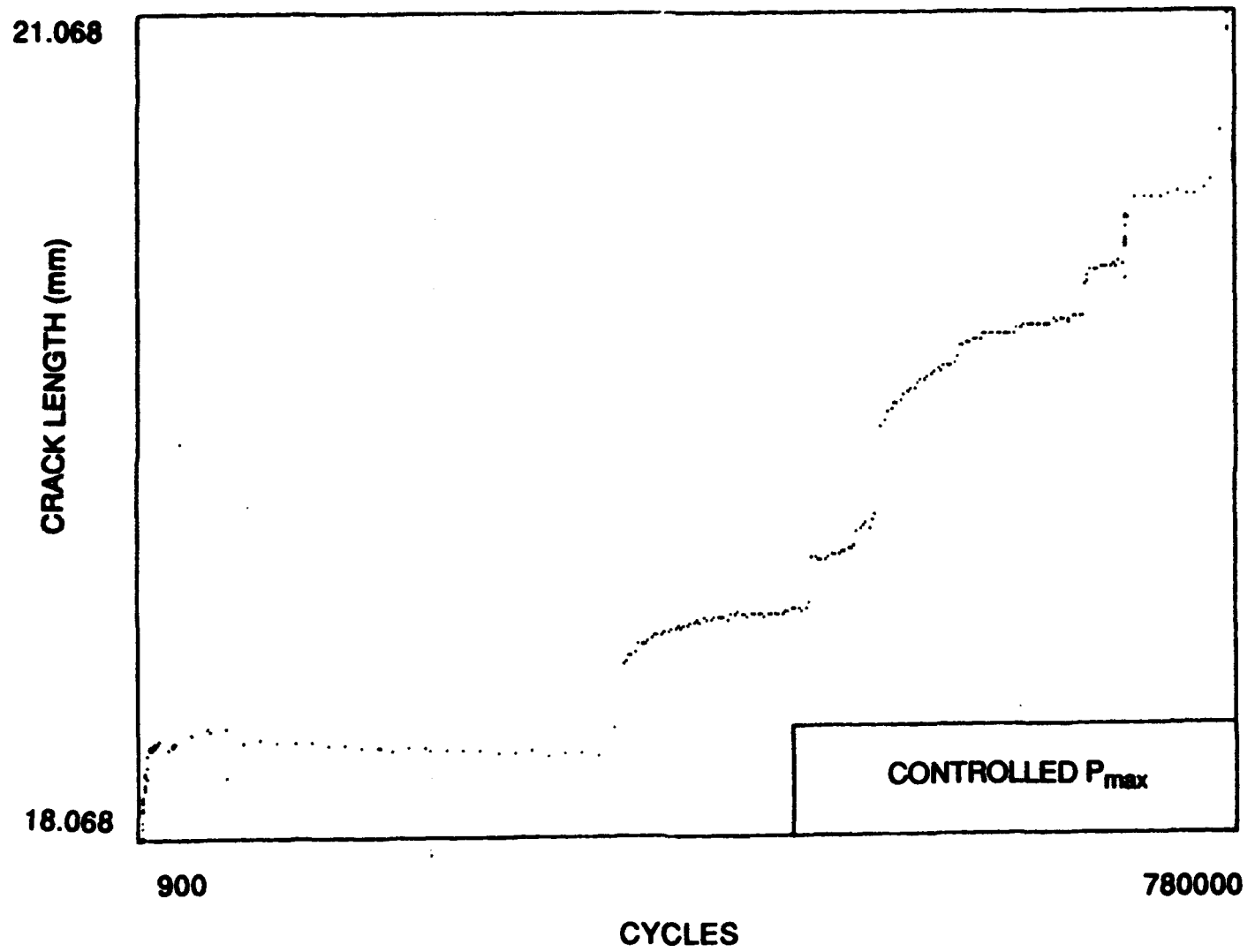

Fig. B1 Fatigue Precracking History for 88C23-6 Standard C(T) Specimen

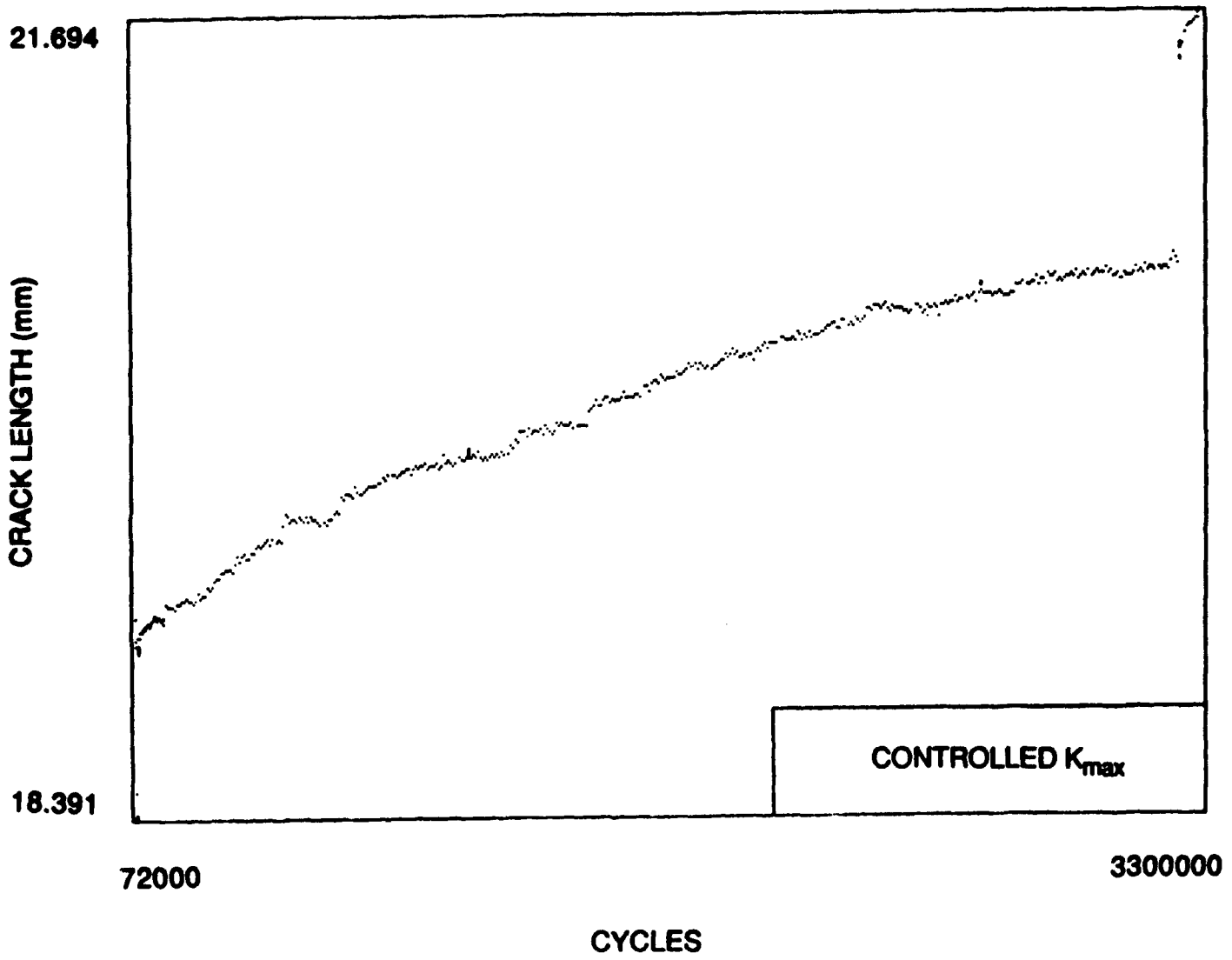

Fig. B2 Fatigue Precracking History for 89C03-9 Standard C(T) Specimen

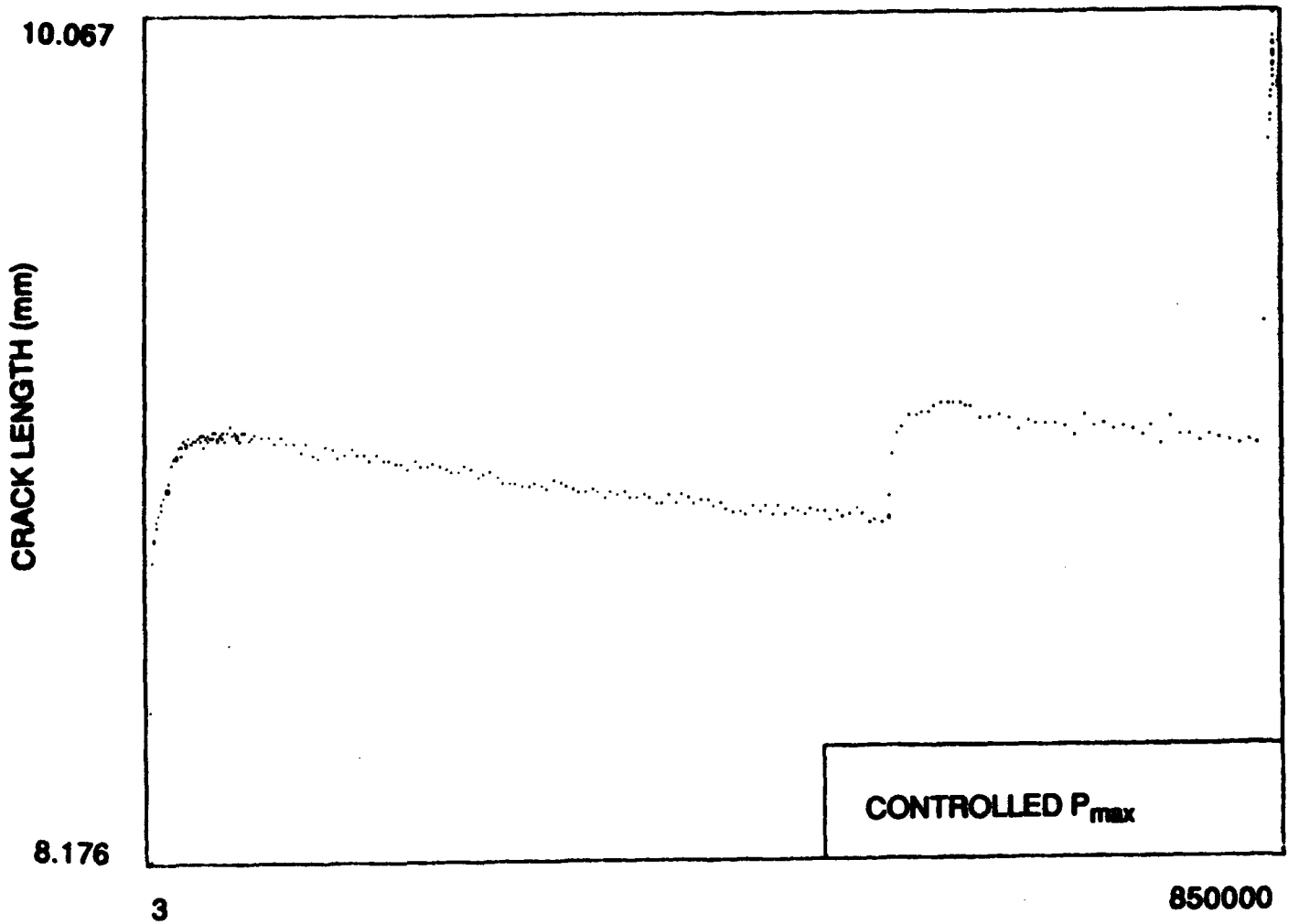

Fig. B3 Fatigue Precracking History for 89C03-3 Mini C(T) Specimen

greater than 21 MPa$\sqrt{m}$, the crack propagated rapidly until final precrack size was reached. For the mini C(T) specimen, 89C03-3, crack retardation at constant load was even observed. When the stress intensity was increased to greater than 20 MPa$\sqrt{m}$, rapid crack propagation occurred in a discrete manner after a few more cycles (Fig B3).

In all three of these specimens, it was observed that frequency affected the compliance crack length. When the frequency was decreased, the compliance crack length increased, although data were acquired at the same frequency of 1 Hz in both cases. When the frequency was changed back to its original high frequency, previous crack length estimates were recovered. This observation is contradictory to what is seen for metals.

APPENDIX C

LOAD-DISPLACEMENT TRACES

Load-diplacement curves for nine specimens are presented in this order:

1) Mini C(T) specimens with diamond-saw notch extensions: 89C03-2, 89C03-4, 89C03-5 (Figures C1, C2, and C3)

2) Mini C(T) specimens with abrasive water-jet notch extensions: 89C03-7 and 89C03-8 (Figures C4 and C5)

3) Standard C(T) specimens with precracking: 88C23-6 and 89C03-9 (Figures C6 and C7)

4) Standard C(T) specimens with abrasive water-jet notch extensions: 88C23-7 and 89C03-10 (Figures C8 and C9)

5) Two load-displacement plots are presented in the text: 89C03-3 and 88C23-4 (Figures 11 and 12)

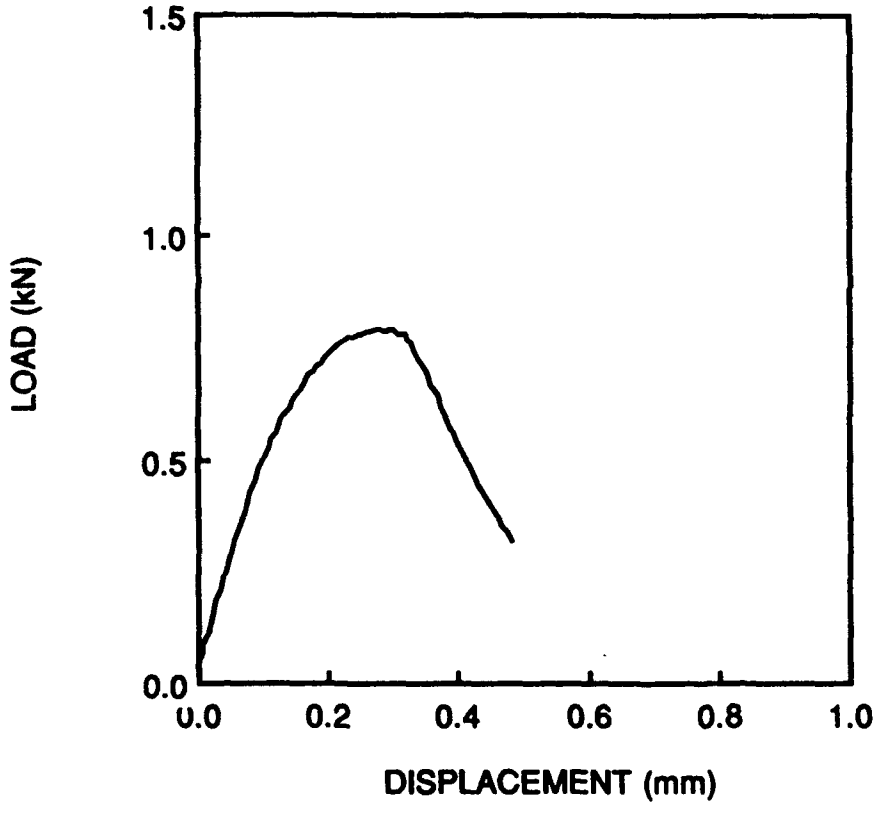

Fig. C1 Load Displacement Behavior of Specimen 89C03-2 (Mini, Diamond-Saw, a/W = 0.52)

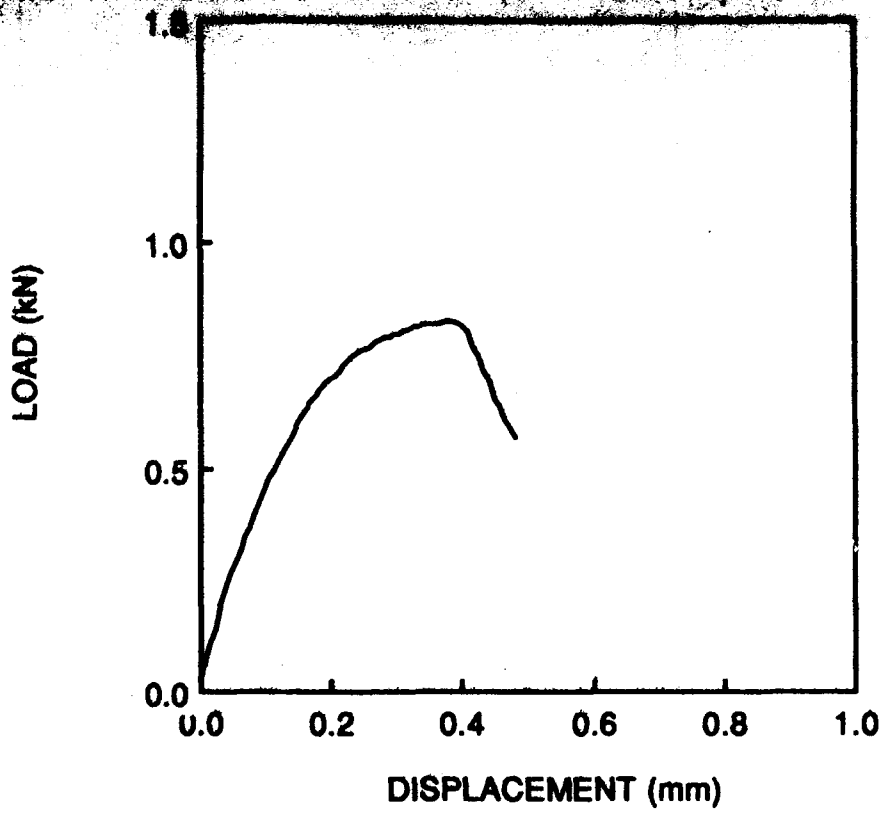

Fig. C2 Load Displacement Behavior of Specimen 89C03-4 (Mini, Diamond-Saw, a/W = 0.52)

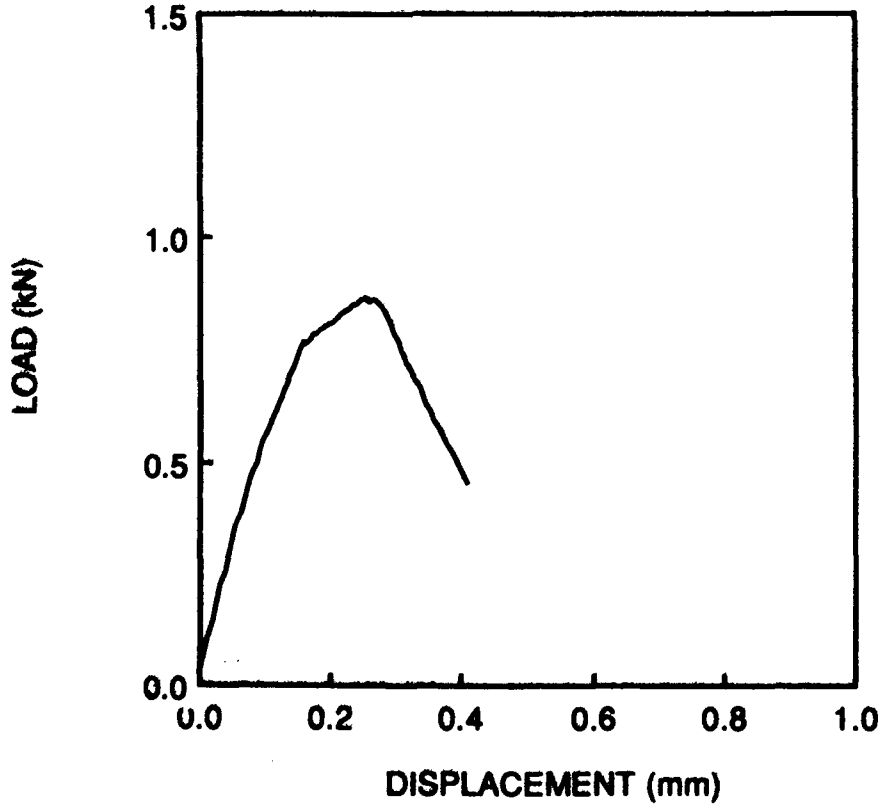

Fig. C3 Load Displacement Behavior of Specimen 89C03-5 (Mini, Diamond-Saw, a/W = 0.50)

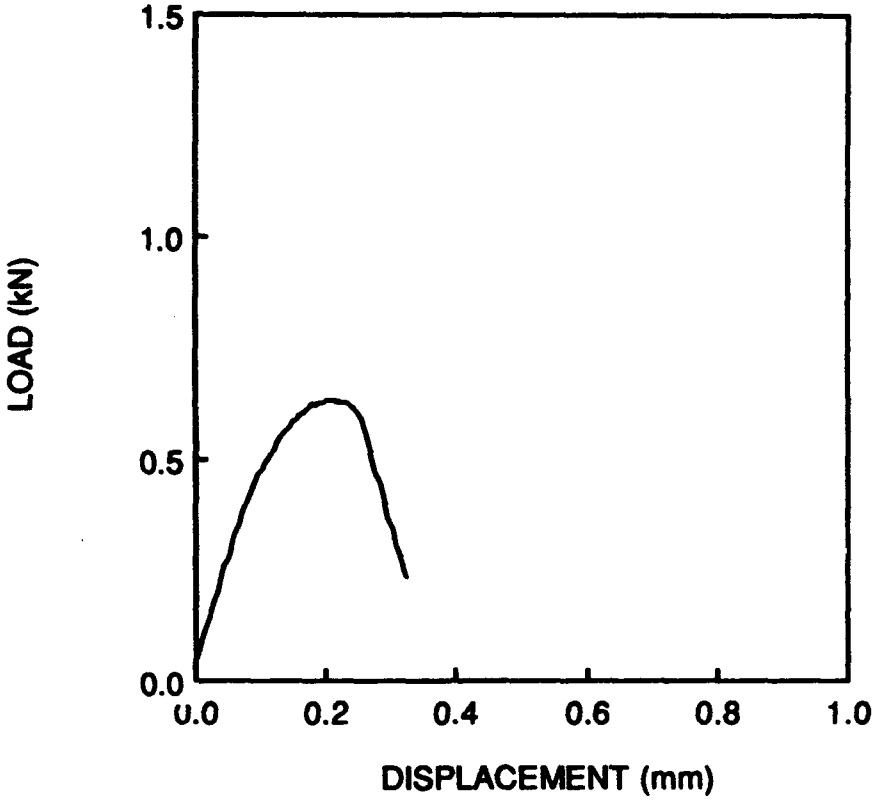

Fig. C4 Load Displacement Behavior of Specimen 89C03-7 (Mini, Water-Jet, a/W = 0.51)

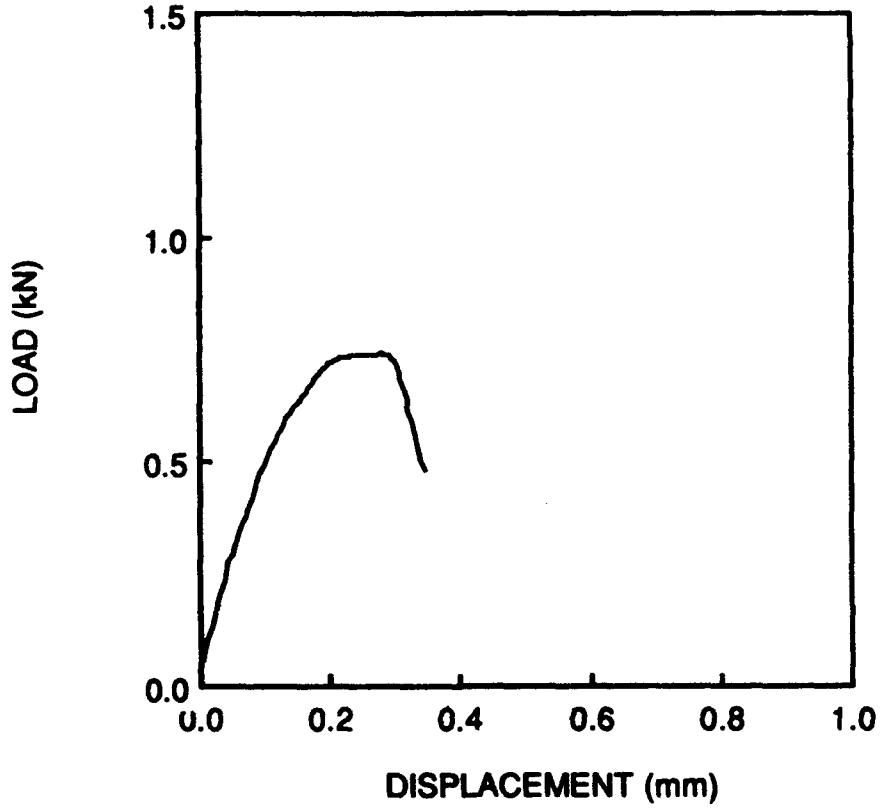

Fig. C5 Load Displacement Behavior of Specimen 89C03-8 (Mini, Water-Jet, a/W = 0.50)

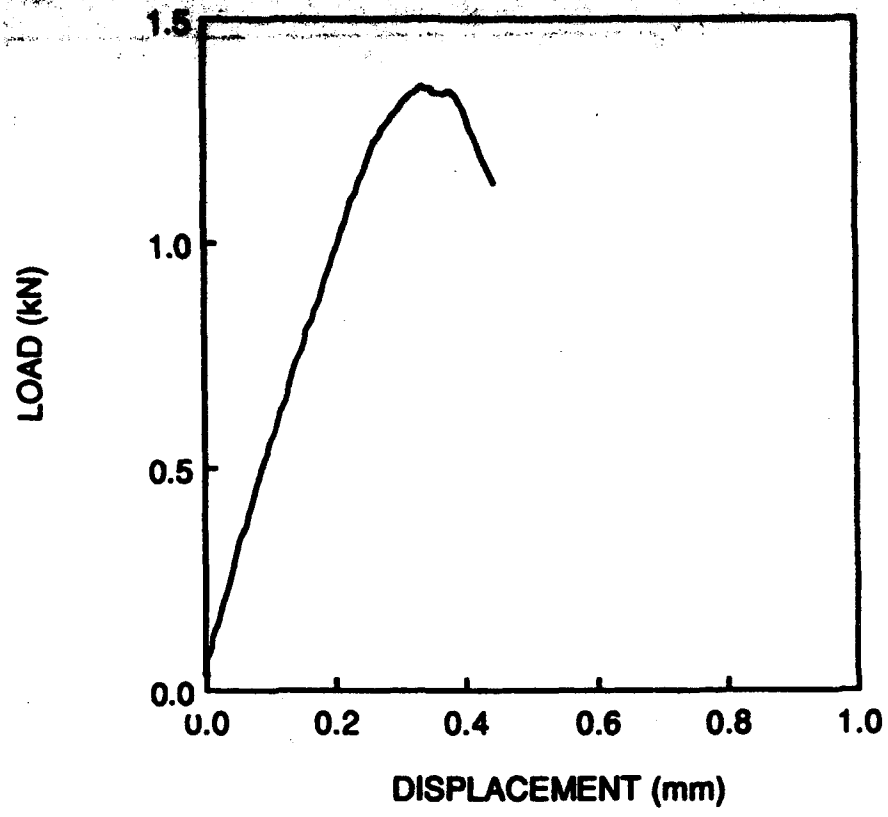

Fig. C6 Load Displacement Behavior of Specimen 88C23-6 (Standard, Precracked, a/W = 0.53)

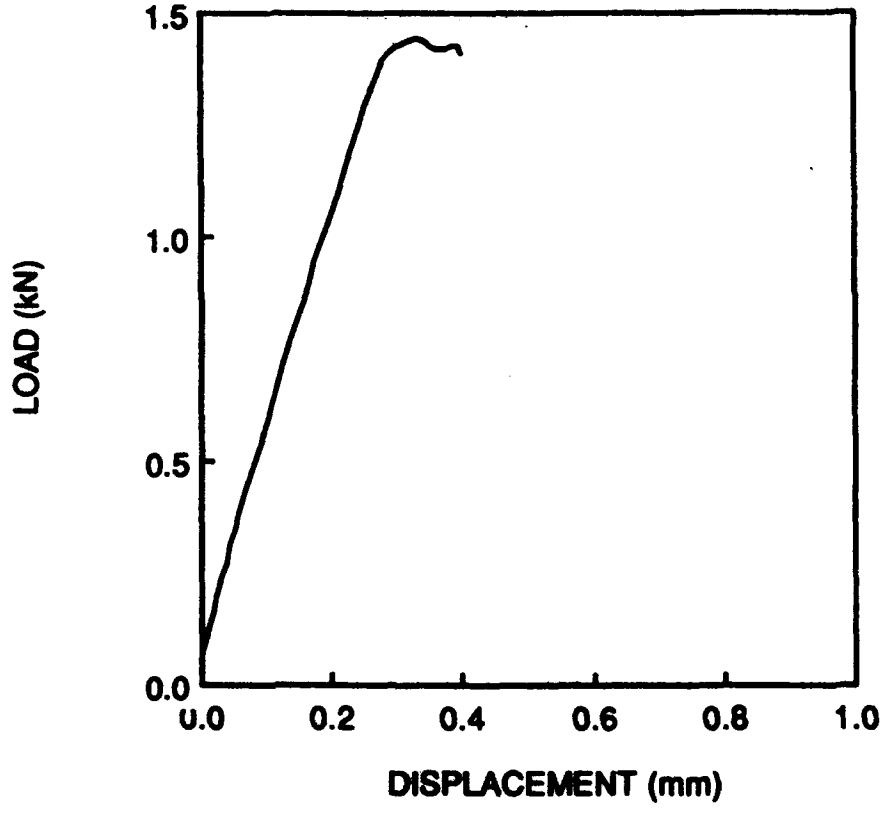

Fig. C7 Load Displacement Behavior of Specimen 89C03-9 (Standard, Precracked, a/W = 0.54)

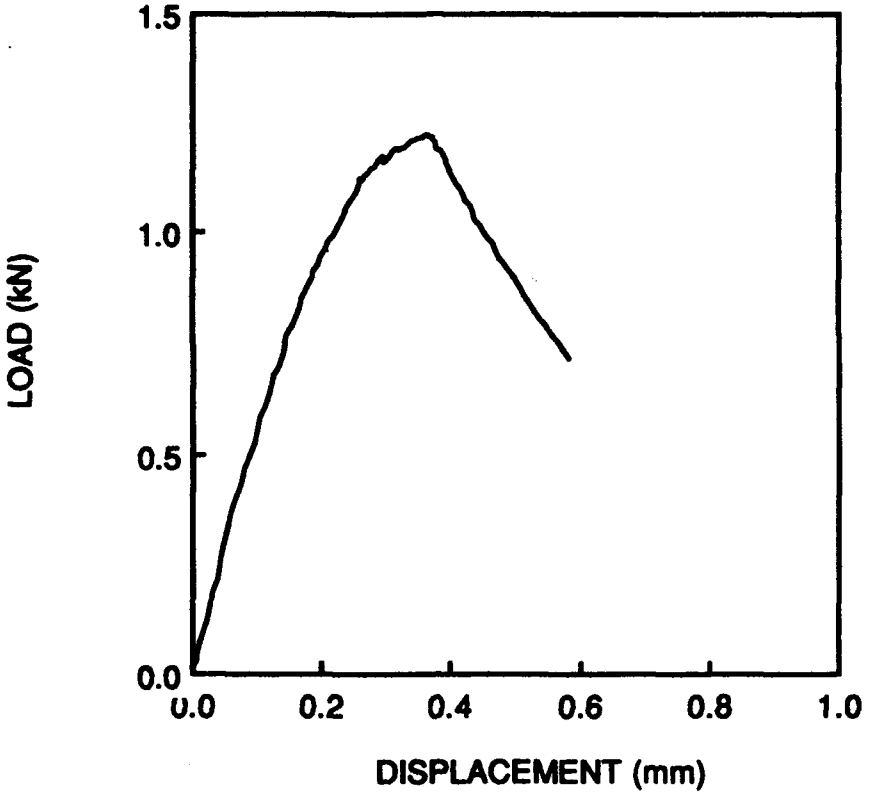

Fig. C8 Load Displacement Behavior of Specimen 88C23-7 (Standard, Water-Jet, a/W = 0.50)

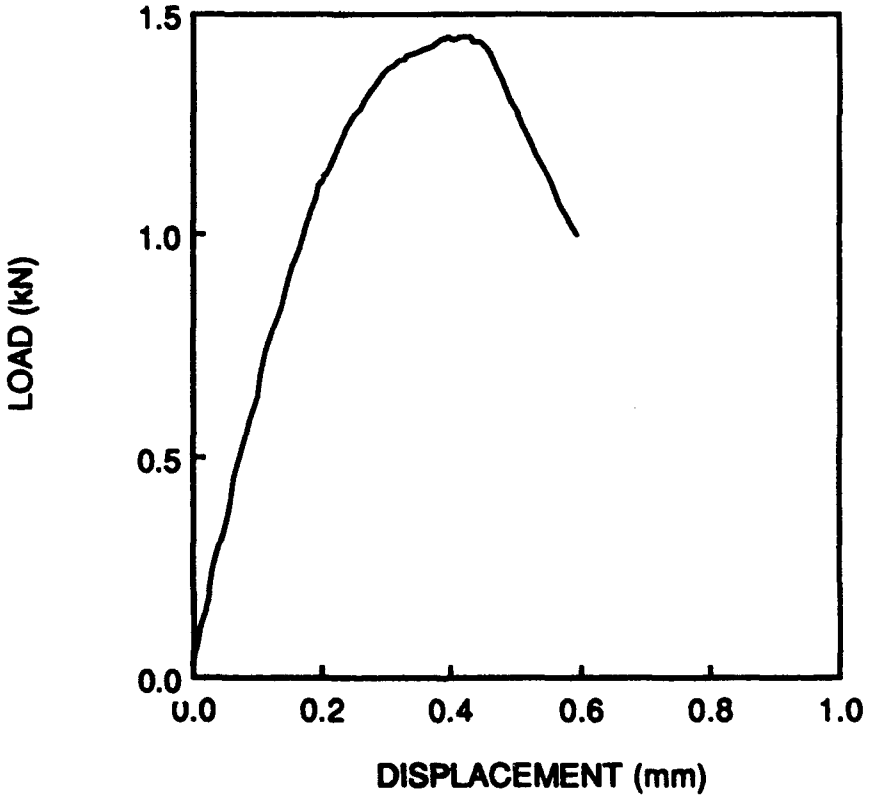

Fig. C9 Load Displacement Behavior of Specimen 89C03-10 (Standard, Water-Jet, a/W = 0.50)

☆ U.S. Government Printing Office:1992—648-127/62363